16. Legged Robots

Shuuji Kajita, Bernard Espiau

In this chapter, we introduce legged robots. After introducing the history of legged robot research in Sect. 16.1, we start to discuss hopping robots and analyze a simple passive walker as a typical cycling walking robot in Sect. 16.2; the Poincaré map is one of the most important tools to analyze its dynamics and stability. In Sect. 16.3, the dynamics and control of general biped robots are discussed. The key is the forward dynamics subject to the unilateral constraint between the feet and the ground. Its formal treatment leads to walking trajectory generation and various control methods. As a practical scheme to control biped robots, we discuss the zero-moment point (ZMP) in Sect. 16.4, including its definition, physical meaning, measurement, calculation, and usage. In Sect. 16.5, we move to multilegged robots. In this field, the most important subject is the relationship between gaits and stability. We also introduce the landmark robots in this field. In Sect. 16.6, we overview the divergence of the legged robots. We see leg–wheel hybrid robots, leg–arm hybrid robots, tethered walking robots, and wall-climbing robots. To compare these legged robots with different configurations, we use some useful performance indices such as the Froude number and the specific resistance, which are introduced in Sect. 16.7. We conclude the chapter and address future trends in Sect. 16.8.

The idea of designing and realizing artificial entities is almost as old as humanity. After some wonderful formal studies by Leonardo Da Vinci, the first notable artificial machines, called *automatons* were built, among others by Jacquard, Jacquet-Droz, Vaucanson (including his famous duck) mainly in France around the 18th century. This was followed by a florilegium of realizations from 1850 to World War I. The area then experienced a long

eclipse, up to the early 1970s. It should be noticed that the revival was then driven by scientists, instead of the brilliant engineers, artists or magicians of the previous centuries.

16.1 A Brief History

The pioneering works in the field of legged robots were achieved around 1970 by two famous researchers, Kato and Vukobratovic. Both works were characterized by the design of relevant experimental systems. In Japan, the first anthropomorphic robot, WABOT 1, was demonstrated in 1973 by I. Kato and his team at Waseda University. Using a very simple control scheme, it was able to realize a few slow steps in static equilibrium. This achievement was the starting point of a prolific generation of legged robots in Japan.

In parallel, M. Vukobratovic and his team were very involved in the problems generated by functional rehabilitation. At the Mihailo Puppin Institute, Belgrade, Yugoslavia, they designed the first active exoskeletons, and several other devices such as the *Belgrade's hand*, but the most well-known outcome remains their analysis of locomotion stability, which exhibited around 1972 the concept of zero-moment point (ZMP), widely used since that time [16.3]. This was the first attempt to formalize the need for dynamical stability of legged robots; the idea was to use the dynamic wrench in order to extend a classical criterion of static balance (the center of mass should project inside the convex hull of contact points). This important point will be detailed later in this Chapter.

In the next decade, the breakthroughs came from the United States. Following the early work of R. McGhee in the 1960s at USC (University of Southern California), then in the 1970s at OSU (Ohio State University), which resulted in the first computer-controlled walking machine, M. Raibert started to study dynamically stable running at CMU (Carnegie Mellon University). Then, he launched the Massachusetts Institute of Technology (MIT) LegLab, where a sequence of active hopping robots, with one, two or four legs were designed, with impressive results, among them a famous flip performed by a two-legged hopping machine. Simultaneously, R. McGhee and K. Waldron, after the building of some prototypes, achieved the design of the largest hexapod in the world, called the *adaptive suspension vehicle*, a quasi-industrial system able to walk on natural irregular terrain, which was driven by a human (Sect. 16.5.2).

A third key period for research in legged robots was the early 1990s. Indeed, the idea of studying purely passive mechanical systems was pioneered by *McGeer* [16.4]. In this seminal paper, McGeer introduces the concept of natural cyclic behavior, for a class of very simple systems: a plane compass on an inclined plane. Stable walking results from the balance between increase of the energy due to the slope and loss at the impacts. However, what should be emphasized here is that McGeer popularized for roboticists the analysis of such systems in terms of orbital stability using Poincaré maps. Several researchers have followed the tracks open by McGeer, with many extensions (examples in Fig. 16.1): adding trunk, feet and knees [16.1], semipassive control, walking/running underactuated systems like the Rabbit robot [16.2], etc.

Finally, the end of the millennium was a period of intense technological activities. Industrial breakthroughs showed to the world that building true humanoids was now possible. In Japan, the first humanoid robot, P2, was exhibited by Honda in 1996, followed by several more. Presently, the most impressive technical achieve-

Fig. 16.1a,b Underactuated biped robots [16.1, 2]

ments are still realized by industrial companies: ASIMO (Honda), QRIO (Sony), HRP (Kawada), being the major examples today, among others. In parallel, it should be noticed that the market for small humanoid robots, mainly aimed at entertainment, has grown steadily over the last decade.

While examining the history above and the present state of the art, it is clear that roboticists are now facing a challenge. Very nice technological achievements are available, especially biped robots. However, the ability of these systems to walk truly autonomously on uneven and various terrains in a robust way, i. e., in daily life, remains to be demonstrated. The goal of this chapter is therefore to provide some keys in modeling and recent control advances, in order to be able to design adequate and efficient control schemes when needed. This will be based on two main classes of approaches: the use of so-called forward dynamics on one hand, and the use of the ZMP on the other hand. The Chapter is organized as follows: after a brief summary of the control principles used for hopping and passive robots, we will focus on the issues needed for the control of biped robots from a dynamic model scheme: modeling aspects, stability issues, trajectory generation, and control. Then we will present in depth the concept of ZMP and its use in a control scheme. Since the first parts are mainly concerned with biped robots, the chapter will end with a section dedicated to multilegged robots.

16.2 Analysis of Cyclic Walking

16.2.1 A Few Points About Hopping Robots

Cyclic legged robots are those that reach, either naturally or with the help from a control, a steady-state behavior characterized by a cycle in the phase plane. The underlying assumption is that there exists in some sense a more or less hidden set of optimal natural behaviors of the system. Within this class, hopping (or bouncing) robots are interesting since they are generally unstable, but capable of high performance in terms of velocities.

As mentioned, these robots have been widely studied in the MIT LegLab. It is not the goal of the Chapter to develop in depth the related design approaches and control techniques, and we refer the reader to the excellent, although ancient, book by *Mark Raibert* [16.5] on the subject. Let us just give a flavor of Raibert's results, taken from this reference.

a) 3D one-leg hopper (1983) **b)** 3D biped (1989)

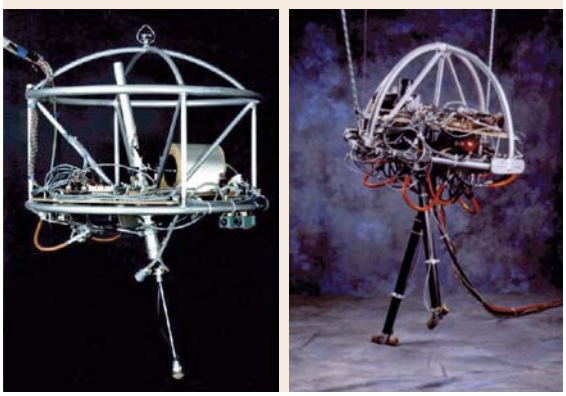

Fig. 16.2a,b Raibert's hopping robots [16.5]

The basis of the work is in fact the planar one-leg hopping robot. Raibert proved that the control of such system could be split into three separate components: the first controls the altitude by providing a fixed thrust during each cycle; the second part controls the forward velocity of the whole system by assigning to the foot, at each step, a given distance from the hip when landing; and the last one controls the body attitude by servoing the hip during the stance phase. The related algorithms are quite simple and allow a real-time implementation. What is very interesting is that this simple approach applies almost straightforwardly to the case of the three-dimensional (3-D) one-legged hopping robot (Fig. 16.2b), and moreover this three-part control scheme can also be extended to biped (Fig. 16.2a) or quadruped robots by adding techniques of leg sequencing and using the concept of a virtual leg when pairs of legs operate in unison.

Indeed, this interesting piece of work was not really followed up, but was surely the inspiration for many researches on cyclic systems. Among these, purely passive walkers have largely been considered, and we will now provide some insight into this area.

16.2.2 Stability of Passive Walking

The aim of this section is to present some basic facts and concepts related to passive walking. Many more details may be found in the literature, for example

in [16.1, 4, 6] among others. The issues considered here are mainly taken from [16.7]. We use the simplest possible model (Fig. 16.3), an unactuated symmetric planar compass descending a slope of angle $\boldsymbol{\phi}$. Masses are pinpoint, and telescopic massless legs are only a way of ensuring foot clearance. Several assumptions underlie the model. Among these, let us mention that the swing phase is assumed to be slipless, and that the double stance phase, during which the swing and support leg are exchanged, is instantaneous. The related impact is slipless and inelastic. We define (following the notation in Fig. 16.3):

$$\begin{cases} \mu = \frac{m_{\mathrm{H}}}{m} \; ; \; \beta = \frac{b}{a} \\ \boldsymbol{x} = [\boldsymbol{q}, \dot{\boldsymbol{q}}]^{\top} = [q_{\mathrm{ns}}, q_{\mathrm{s}}, \dot{q}_{\mathrm{ns}}, \dot{q}_{\mathrm{s}}]^{\top} \; . \end{cases} \tag{16.1}$$

The swing-stage equations of the robot, similar to those for a frictionless double pendulum, can be written in the form of Lagrangian dynamics

$$\boldsymbol{H}(\boldsymbol{q})\ddot{\boldsymbol{q}} + \boldsymbol{C}(\boldsymbol{q}, \dot{\boldsymbol{q}})\dot{\boldsymbol{q}} + \frac{1}{a}\boldsymbol{\tau}_{\mathrm{g}}(\boldsymbol{q}) = 0 \; , \tag{16.2}$$

where

$$\boldsymbol{H}(\boldsymbol{q}) = \begin{pmatrix} \beta^2 & -(1+\beta)\beta\cos 2\alpha \\ -(1+\beta)\beta\cos 2\alpha & (1+\beta)^2(\mu+1)+1 \end{pmatrix} ,$$

$$\boldsymbol{C}(\boldsymbol{q}, \dot{\boldsymbol{q}}) = \begin{pmatrix} 0 & \\ -(1+\beta)\beta\dot{q}_{\mathrm{ns}}\sin(q_{\mathrm{s}} - q_{\mathrm{ns}}) & \\ (1+\beta)\beta\dot{q}_{\mathrm{s}}\sin(q_{\mathrm{s}} - q_{\mathrm{ns}}) & \\ 0 & \end{pmatrix} ,$$

$$\boldsymbol{\tau}_{\mathrm{g}}(\boldsymbol{q}) = \begin{pmatrix} g\beta\sin q_{\mathrm{ns}} \\ -[(\mu+1)(1+\beta)+1]g\sin q_{\mathrm{s}} \end{pmatrix} ,$$

where 2α is the inter-leg hip angle.

The specificity of this system with respect to, for example, manipulation robots, is that we have to complete the continuous dynamics with equations describing the step transition. We will encounter this requirement of separate modeling in legged locomotion again when presenting the dynamics of bipedal walking (Sect. 16.3.2).

The pre- and the post-impact configurations of the robot can be related by $\boldsymbol{q}^{+} = \boldsymbol{S}\boldsymbol{q}^{-}$, where $\boldsymbol{S}$ is a 2×2 antisymmetric matrix with unit elements. The principle of conservation of angular momentum applied to the robot gives $\boldsymbol{Q}^{-}(\alpha)\dot{\boldsymbol{q}}^{-} = \boldsymbol{Q}^{+}(\alpha)\dot{\boldsymbol{q}}^{+}$, from

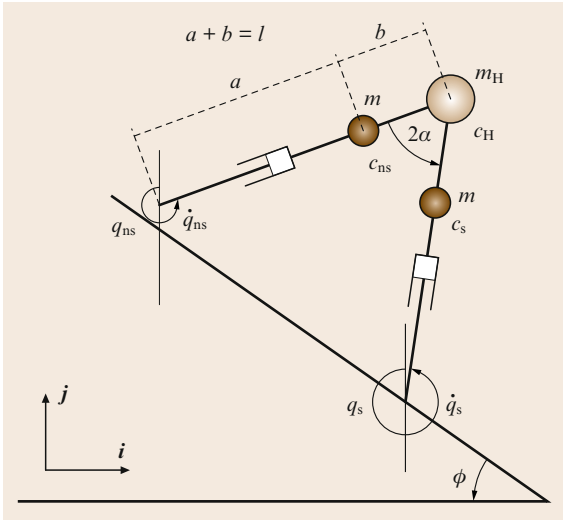

Fig. 16.3 Compass model

which we can obtain the joint velocity relationship $\dot{\boldsymbol{q}}^{+} = [\boldsymbol{Q}^{+}(\alpha)]^{-1}\boldsymbol{Q}^{-}(\alpha)\dot{\boldsymbol{q}}^{-} = \boldsymbol{A}(\alpha)\dot{\boldsymbol{q}}^{-}$, where

$$\boldsymbol{Q}^{-}(\alpha) = \begin{pmatrix} -\beta & -\beta + [\mu(1+\beta)^2 + 2(1+\beta)]\cos 2\alpha \\ 0 & -\beta \end{pmatrix} ,$$

$$\boldsymbol{Q}^{+}(\alpha) = \begin{pmatrix} \beta[\beta - (1+\beta)\cos 2\alpha] & \\ & \beta^2 \\ (1+\beta)[(1+\beta) - \beta\cos 2\alpha] & \\ \cdots + 1 + \mu(1+\beta)^2 & \\ -\beta(1+\beta)\cos 2\alpha & \end{pmatrix} .$$

The complete state vector $\boldsymbol{x}$ before and after impact can thus be written as

$$\boldsymbol{x}^{+} = \boldsymbol{W}(\alpha)\boldsymbol{x}^{-} \tag{16.3}$$

with matrix $\boldsymbol{W}(\alpha) = \begin{pmatrix} \boldsymbol{S} & 0 \\ 0 & \boldsymbol{A}(\alpha) \end{pmatrix}$.

The periodic dynamic behavior of this system can be summarized in the phase portrait given in Fig. 16.4, where discontinuities result from impacts. The stability of this system can be analyzed in terms of *orbital stability*, a theoretical definition of which can be found in [16.7]. Intuitively, this means that, when the system deviates from its trajectory in the phase plane within a certain domain (the basin of attraction), its natural be-

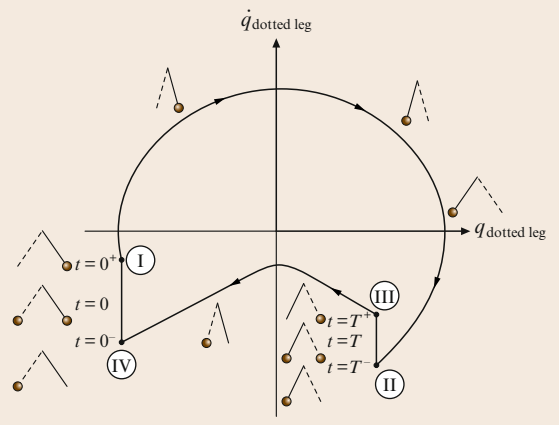

Fig. 16.4 Typical cycle

havior is to return to this phase-plane trajectory, called the limit cycle.

The concept of orbital stability is well suited to the analysis of cyclic systems such as steady-state walking. Thus, the robustness of the obtained gait can be assessed by measuring the size of the basin of attraction. However, for a general nonlinear system, the proof of the existence of a limit cycle, the analysis of its local orbital stability, and the procedure to compute the cycle and its basin of attraction are often difficult. For example, in the present case, the analysis would require the explicit integration of the dynamics during the swing phase. Nevertheless, it is possible to test the local stability of a limit cycle, once it has been found. One method to determine the stability of the robot gait is through the numerical computation of its Poincaré map [16.4]. Limit cycles are fixed points of this map, which in the context of biped locomotion is called the *stride function* [16.4]. Essentially the procedure consists of injecting small perturbations to the robot states around the limit cycle and calculating the eigenvalues of the sensitivity matrix. For an orbitally stable cycle the eigenvalues lie within the unit circle. A natural choice of the Poincaré section corresponds to the state where the swing leg hits the ground. This introduces a natural discretization of the dynamics. For two successive touchdowns of the same leg, the states of the robot are related as:

$$\boldsymbol{x}_k = \boldsymbol{F}(\boldsymbol{x}_{k+1}) \,. \tag{16.4}$$

The equilibrium is the solution of $\boldsymbol{x}^* = \boldsymbol{F}(\boldsymbol{x}^*)$. By taking a first-order expansion, we have

$$\boldsymbol{F}(\boldsymbol{x}^* + \Delta\boldsymbol{x}^*) \approx \boldsymbol{x}^* + (\nabla\boldsymbol{F})\Delta\boldsymbol{x}^* . \tag{16.5}$$

Therefore, $(\nabla\boldsymbol{F})\Delta\boldsymbol{x}^* \approx \boldsymbol{F}(\boldsymbol{x}^* + \Delta\boldsymbol{x}^*) - \boldsymbol{x}^*$, and a numerical procedure can be used to check whether the moduli of the eigenvalues of $(\nabla\boldsymbol{F})$ are strictly less than 1. One method is to apply successively smaller perturbations to every state and observe their first-return map, then to numerically solve the equation $(\nabla\boldsymbol{F})\boldsymbol{\tau} = \Psi$, where the 4×4 diagonal matrix $\boldsymbol{\tau}$ collects the state variable perturbations and Ψ the measured variations in the first-return map. Note that this method is quite general and can be applied to other kind of mechanical systems that exhibit a periodic behavior.

It has been shown that passive walking robots can exhibit stable limit cycles. Often, for a given slope, ϕ, and for a particular range of slopes, the number of such stable behaviors is one. Interestingly, increasing ϕ may lead to the appearance of period doubling, evolving towards a chaotic behavior if ϕ is too large (Fig. 16.5).

In conclusion, it should be emphasized that this class of machines has inspired the design of efficient simple biped robots. Indeed, systems that exhibit natural passive gaits are *optimal* in some energetic sense. A limit cycle is analogous to the comfortable walking gait of humans, in which the consumption of metabolic energy per unit distance is minimal. An interesting idea is therefore to add to a passive system a minimum set of actuators in order to just compensate for the loss of energy when the system is not on a descending slope. Several laboratory realizations are based on this principle, but this idea has yet to be exploited for operational legged robots.

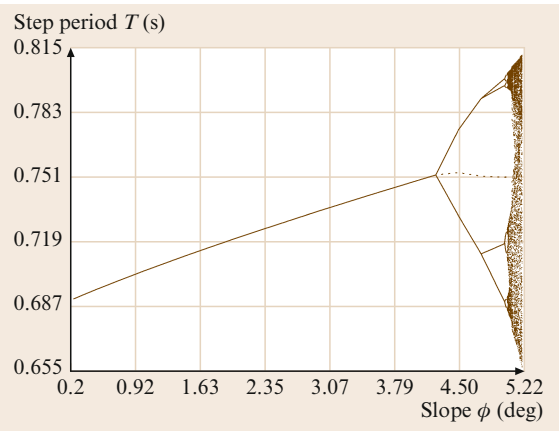

Fig. 16.5 Bifurcations and chaos

16.3 Control of Biped Robots Using Forward Dynamics

This section presents a view of the state of the art in modeling and control of biped robots in the framework of forward dynamics. Space does not allow to go deeply into the details of the equations or their derivation, which is why we only provide the reader with the essential issues and refer to more complete papers, such as [16.8, 9] and mainly the deep analysis of [16.10, 11].

16.3.1 Configuration Space

A biped robot is usually modeled as a rigid tree-form tridimensional articulated structure. Basically, the internal parameterization is q_1, while that of the joint space is Q. If the robot is considered as having its foot (resp. feet) motionless during every phase of swing (resp. stance), then the model is that of a classical robot manipulator. If all joints are actuated, then the closure equations make the robot overactuated during the stance phase (with two feet on the ground). However, it is more correct and general to consider a walking robot as a free system in space, but subject to nonconstant unilateral contacts. The configuration space is therefore $\{\{Q\} \oplus R^3 \oplus SO(3)\}$, where the six-dimensional (6-D) displacement of a given body is parameterized by q_2.

16.3.2 Dynamics

A basic modeling approach consists of splitting the dynamics equations into three parts: Lagrangian dynamics in the full space; constraints due to contact forces; and transition equations with impacts.

Continuous Dynamics and Contact Forces

Under the assumption that the robot structure is rigid, continuous dynamics can be expressed in the Lagrangian form

$$\boldsymbol{H}(\boldsymbol{q})\ddot{\boldsymbol{q}} + \boldsymbol{C}(\boldsymbol{q},\dot{\boldsymbol{q}})\dot{\boldsymbol{q}} + \boldsymbol{G}(\boldsymbol{q}) = \boldsymbol{\Gamma} + \boldsymbol{\Gamma}_{\text{ext}} \,, \tag{16.6}$$

where $\boldsymbol{q} = (\boldsymbol{q}_1, \boldsymbol{q}_2) \in \mathcal{R}^n$ is defined in Sect. 16.3.1. $\boldsymbol{\Gamma} = [0, \boldsymbol{\tau}]^\top \in \mathcal{R}^n$ is the generalized efforts vector, including the joint actuation torques (generally bounded), $\boldsymbol{\tau} \in \mathcal{R}^m$; $\boldsymbol{H}$ is the inertia matrix, $\boldsymbol{C}$ is the matrix of centrifugal, gyroscopic, and Coriolis effects, and $\boldsymbol{\tau}_g$ is the generalized gravity force vector. The set $(\boldsymbol{q}, \dot{\boldsymbol{q}})$ constitutes the *state* of the robot.

The points of the robot in contact with the ground satisfy a closure equation of the form

$$\boldsymbol{\phi}(\boldsymbol{q}) = \begin{pmatrix} \boldsymbol{\phi}_n(\boldsymbol{q}) \\ \boldsymbol{\phi}_t(\boldsymbol{q}) \end{pmatrix} = 0 \,,$$

where $\boldsymbol{\Gamma}_{\text{ext}}$ are the torques generated by these ground contact, which can be expressed as

$$\boldsymbol{\Gamma}_{\text{ext}} = \boldsymbol{J}(\boldsymbol{q})^\top \boldsymbol{\lambda}(\boldsymbol{q},\dot{\boldsymbol{q}}) \,,$$

where $\boldsymbol{J}(\boldsymbol{q}) = \frac{\partial \phi(q)^\top}{\partial q}$ is the Jacobian matrix of the contact points of the robot, i. e., where the external forces are applied. $\boldsymbol{\lambda}(\boldsymbol{q},\dot{\boldsymbol{q}})$ are Lagrange multipliers. We can split this expression into two parts

$$\boldsymbol{\Gamma}_{\text{ext}} = \boldsymbol{J}_n(\boldsymbol{q})^\top \boldsymbol{\lambda}_n(\boldsymbol{q},\dot{\boldsymbol{q}}) + \boldsymbol{J}_t(\boldsymbol{q})^\top \lambda_t(\boldsymbol{q},\dot{\boldsymbol{q}}) \,.$$

The subscripts 'n' and 't' stand for normal and tangential to the ground components, respectively. The Lagrange multipliers $\boldsymbol{\lambda}_n$ and $\boldsymbol{\lambda}_t$ express the amplitudes of those efforts.

Now, there are two main ways of modeling the ground interaction. First, it is possible to consider a viscoelastic model, but this suffers from possible problems in the physical analysis and numerical integration. We will consider here the opposite case: that the contacts are rigid and result in a set of constraints, called unilateral, such as nonpenetration, to which should be added a friction model. The semipositive normal forces and accelerations of the contact points are therefore related by a complementarity condition [16.10, 12]

$$\boldsymbol{\lambda}_n^\top(\boldsymbol{q},\dot{\boldsymbol{q}})\ddot{\boldsymbol{\phi}}_n(\boldsymbol{q}) = 0, \boldsymbol{\lambda}_n(\boldsymbol{q},\dot{\boldsymbol{q}}) \geq 0, \ddot{\boldsymbol{\phi}}_n(\boldsymbol{q}) \geq 0 \,.$$

Excluding the case where the system is slipping, tangential constraints can be written as

$$\ddot{\boldsymbol{\phi}}_t(\boldsymbol{q}) = 0 \,.$$

Finally, since the existence of friction limits the allowed tangential forces, a nonslip condition is satisfied as long as

$$\|\boldsymbol{\lambda}_t\| \leq \boldsymbol{\mu}_0 \boldsymbol{\lambda}_n \,,$$

where μ_0 is the friction coefficient, which depends on the materials in contact.

Impacts

As stated in Sect. 16.2.2, if the impact is assumed to be inelastic and nonsliding, the velocity of the system jumps from $\dot{\boldsymbol{q}}^-$ to $\dot{\boldsymbol{q}}^+$ according to the equations

$$\boldsymbol{H}(\boldsymbol{q})(\dot{\boldsymbol{q}}^+ - \dot{\boldsymbol{q}}^-) = \boldsymbol{J}_n(\boldsymbol{q})^\top \boldsymbol{\Lambda}_n(\boldsymbol{q},\dot{\boldsymbol{q}}) + \boldsymbol{J}_t(\boldsymbol{q})^\top \boldsymbol{\Lambda}_t(\boldsymbol{q},\dot{\boldsymbol{q}}) \,,$$

where $\boldsymbol{\Lambda}(\boldsymbol{q},\dot{\boldsymbol{q}}) = [\boldsymbol{\Lambda}_n(\boldsymbol{q},\dot{\boldsymbol{q}}), \boldsymbol{\Lambda}_t(\boldsymbol{q},\dot{\boldsymbol{q}})]^\top$ is the vector of the impulse forces.

Under the assumption that contact points do not move after impact, we can write:

$$\dot{\boldsymbol{\phi}}_{\mathrm{n}}(q) = \boldsymbol{J}_{\mathrm{n}}(\boldsymbol{q})\dot{\boldsymbol{q}}^{+} = 0 \quad \text{and} \quad \dot{\boldsymbol{\phi}}_{\mathrm{t}}(\boldsymbol{q}) = \boldsymbol{J}_{\mathrm{t}}(\boldsymbol{q})\dot{\boldsymbol{q}}^{+} = 0$$

Dynamic Balance

Basically, a biped robot is in equilibrium if it maintains a walk without falling. In the early times of robotics, the gaits were *statical*. This means that, when the velocities and accelerations are small, and assuming that contact points are motionless during each phase of the step, the balance condition reduces to the classical one: the projection of the robot's center of mass belongs to the convex hull of contact points. Therefore, a static walk can be defined as a continuous sequence of configurations ensuring the forward progression and maintaining the erected position of the system simultaneously such that at each instant the static equilibrium condition is satisfied. As we will see later, related control schemes are easy to design.

However, the true interesting issue is dynamic balance. Nicely addressed in the case of Raibert's hopping robots or for passive walkers through orbital stability as presented in Sect. 16.2.2, the questions of stability and balance deserve a deeper analysis in the case of other kinds of biped robots, such as the work described in [16.11].

For a biped robot, *the dynamical equilibrium can be intuitively linked to the idea of a possible movement*. Let us firstly return to the dynamics; splitting the equations in a way coherent with the two parts of the configuration space, the dynamics (16.6) can be rewritten as:

$$\begin{cases} \boldsymbol{H}_1(\boldsymbol{q})\ddot{\boldsymbol{q}} + \boldsymbol{C}_1(\boldsymbol{q},\dot{\boldsymbol{q}})\dot{\boldsymbol{q}} = \boldsymbol{\tau} + \boldsymbol{J}_1(\boldsymbol{q})^{\top}\boldsymbol{\lambda} - \boldsymbol{\tau}_{g1}(\boldsymbol{q})\,, \\ \boldsymbol{H}_2(\boldsymbol{q})\ddot{\boldsymbol{q}} + \boldsymbol{C}_2(\boldsymbol{q},\dot{\boldsymbol{q}})\dot{\boldsymbol{q}} = \ 0 \ + \boldsymbol{J}_2(\boldsymbol{q})^{\top}\boldsymbol{\lambda} - \boldsymbol{\tau}_{g2}(\boldsymbol{q})\,, \end{cases} \tag{16.7}$$

where $\boldsymbol{\tau}$ is the set of actuator torques.

It can be shown [16.11] that the left-hand side of the second equation of (16.7) is equivalent to the dynamic wrench of the system, while the right-hand side is equivalent to the wrench of contact and gravity forces. This equation is of the Newton–Euler form, where the Newton part can be expressed easily in terms on the acceleration of the center of mass of the robot. This shows a fundamental issue: the global displacement and orientation of the robot can only be realized through contact forces. Moreover, this motion is necessarily associated with a change of posture. More generally, the system can achieve a desired movement if and only if the total wrench of gravity and contact forces is equal to the dynamic wrench of the robot. For a given control scheme, the question is then to check whether this property is satisfied by the robot under control.

In the case where all contact points are in the same plane, it can be shown that there exists a point in this plane around which the horizontal rotation momentum of gravity and dynamic forces vanishes. This point is known as the *zero-moment point* (ZMP), and is also the *center of pressure* (CoP). We will see in Sect. 16.4 how this concept allows the derivation of efficient control schemes.

Another way of setting the problem of the dynamic balance of a walking machine while also taking into account nonhorizontality and tangential forces is to state the problem as follows. A necessary condition for a walking system to realize a motion specified by a trajectory $q(t)$ on a given time interval is that there exists contact forces $\lambda(t)$ such that

$$\begin{cases} \boldsymbol{H}_2(\boldsymbol{q})\ddot{\boldsymbol{q}} + \boldsymbol{C}_2(\boldsymbol{q},\dot{\boldsymbol{q}})\dot{\boldsymbol{q}} + \boldsymbol{\tau}_{g2}(q) = \boldsymbol{J}_2(\boldsymbol{q})^{\top}\boldsymbol{\lambda}\,, \\ \boldsymbol{A}(\boldsymbol{\lambda}) \geq 0\,, \end{cases} \tag{16.8}$$

where the vector inequality $\boldsymbol{A}(\boldsymbol{\lambda}) \geq 0$ gathers all constraints on normal (unilaterality) and tangential (Coulomb friction) forces. Finally, the motion can definitively be achieved if the actuation forces are compatible with the dynamical requirements of the first equation of (16.7). As an illustration of this, we will propose in the next section a control method in relation to this approach.

16.3.3 Trajectory Generation

A frequently used approach for designing a full biped control scheme is to combine the a priori definition of desired trajectories to follow, a classical control allowing them to be tracked, and dedicated online adaption techniques to cope with model uncertainties, obstacles, and disturbances to prevent the robot from falling. Two main classes of methods can be used to compute the desired (also called *reference*) trajectories: they can either be obtained from capturing human motions, or be purely computer generated. In the latter case, the usual approach includes two steps: first, a set of output variables with adequate dimension is chosen. This is generally made from the three-dimensional (3-D) coordinates of a few selected points on the robot. Secondly, after parameterization (under the form of splines, for example) the desired trajectories of these variables are computed for every phase of the gait: stance, swing, left or right, etc.,

allowing one to take into account, for example, obstacles or stairs. They can be either all synchronized in time, or be functions of a single timed reference coordinate. The most interesting way of achieving this computation is to use an optimization algorithm based on the dynamics that takes into account various constraints. The trajectories either remain specified in the output space or are transformed in trajectories in the joint space, $\boldsymbol{q}_\mathrm{d}(t)$. Finally, these trajectories are tracked by a controller, as explained later; an online walk stabilization mechanism is often added.

Another approach to be mentioned is the possibility to use bio-inspired techniques, such as the central pattern generator. The idea is to design self-oscillating systems (i. e., without inputs, although the shape of the output is tunable through some parameters) from which synchronized periodic motions of the joints can be derived. This approach is generally used for generating gaits for multilegged robots (quadrupeds, hexapods) or snake-like systems, but some works also address biped robots [16.13]. The most well-known nonlinear oscillator is the Van der Pol equation

$$\ddot{y} + a(1 - by^2)\dot{y} + c^2 y = 0 \,, \tag{16.9}$$

from which many variations can be derived. Similar results can be obtained from a more biologically inspired point of view, through the design of neural oscillators [16.14]. In this case, sets of artificial neural networks with possible open-loop sinusoidal excitation are connected to generate plausible walking patterns. In some cases it is even possible to create a kind of feedback to cope with environmental variations or to improve stability [16.15].

16.3.4 Control

We present in this subsection three examples of control schemes only, without details. Indeed, many kinds of control schemes are reported in the literature and it is not possible in a single chapter to provide an exhaustive view. We therefore refer the reader to the best journals and conferences in this field for more information [16.16–23].

Simple Dynamic Control

For simplicity, let us only consider the case where the desired walking behavior is specified as a set of multidimensional reference joint trajectories, $\boldsymbol{q}_\mathrm{d}(t)$, defined for every distinct walking phase. It is now necessary to design a control scheme allowing these trajectories to be tracked as accurately as possible in the ideal case. Basically, a proportional–(integral)–derivative (PID) loop on the tracking error is the core of such a control scheme. However, since the use of high gains in a PID controller is not always desirable, due both to the presence of noise and to the need for discretization, good tracking performance require the integration of mechanical modeling issues into the control. When the dynamics of the system are well known, it is often interesting to use them, in a so-called computed torque approach, in which the applied control torque is of the generic form

$$\begin{aligned}\boldsymbol{\Gamma} = {} & \hat{\boldsymbol{H}}(\boldsymbol{q})(k_\mathrm{p}(\boldsymbol{q} - \boldsymbol{q}_\mathrm{d}) + k_\mathrm{v}(\dot{\boldsymbol{q}} - \dot{\boldsymbol{q}}_\mathrm{d}) + \ddot{\boldsymbol{q}}_\mathrm{d}) \\ & + \hat{\boldsymbol{C}}(\boldsymbol{q}, \dot{\boldsymbol{q}})\dot{\boldsymbol{q}} + \hat{\boldsymbol{\tau}}_\mathrm{g}(\boldsymbol{q}) + \hat{\boldsymbol{I}}_\mathrm{F} \,,\end{aligned} \tag{16.10}$$

where, in relation to the dynamics of (16.6), the hats mean that approximate models are used. $\hat{\boldsymbol{I}}_\mathrm{F}$ covers friction aspects and the k_* are control gains. This form is given in the joint space, but can be also used in other diffeomorphic output spaces. Concerning the models, let us note that, at least, the compensation of gravity term $\hat{\boldsymbol{\tau}}_\mathrm{g}(\boldsymbol{q})$ should be considered. Moreover, one of the most important source of errors is the effect of internal friction. As soon as an effective model of friction in joints, gears, and actuators, $\hat{\boldsymbol{I}}_\mathrm{F}$, is available, it should be used, of course with care. In practice, if foot switches exist, phase transitions, leg synchronization, and reinitialization of the trajectories on their cycle can be triggered by the events generated by such sensors (see also Sect. 7.4)

This kind of control can be used at least for generating static walking. If the trajectories have been generated in a dynamical framework, for example, by taking into account a desired position of the ZMP, it can also be used in dynamic walk, possibly with the addition of a dedicated stabilization algorithm. Many variations of this scheme exist based, for example, the linearization of the dynamics, or the use of an inverted-pendulum model.

Nevertheless, although this kind of control can overcome some internal disturbances, it is neither sufficient to ensure the stability of *walking* in a robust enough way in real time, nor able to cope with environmental uncertainties. The basic requirement is now to find a way of controlling the ground contact forces in order to be sure that the support foot (or feet) remain motionless when it is specified and/or needed by the reference trajectory. This means that the control has to ensure that the inequality conditions (no sliding, no take-off), which involve the Lagrange multipliers as stated in Sect. 16.3.2, are verified at each time despite disturbances. Nevertheless, this capacity of reaction will be limited by the bounds that exist on the actuators.

An adequate way of addressing the question of online walk stabilization is to share the control in two parts [16.24, 25]: a first part, which is devoted to the tracking of the prescribed trajectory and involves a large subset of the joints and a second part, dedicated to the control of the ground forces through selected joints (the trunk, or more often, the ankles). It can effectively be shown that controlling ankle torques is a way of approximately control ground reaction forces through an adequate compliant model. Like the similar scheme called *hybrid control* in robot manipulators (see Sect. 7.4), the implementation can use the contact wrenches more or less directly, estimated from force/torque sensors integrated within the ankles or the soles of the feet.

A Variation: The Use of Parameterized Trajectories

A drawback of the classical tracking trajectory approach is that it is necessary to explicitly design as many trajectories as possible situations. Therefore, adaptation to disturbances requires a jump from one trajectory to another, for example, in order to stride over a small obstacle or when it is required to increase or lower the overall velocity by modifying the shape, duration, and length of the prescribed step. An interesting attempt to derive a systematic way of online adaption of the behavior of the system consists of adding degrees of freedom to the definition of the trajectories to be tracked by parameterizing them [16.26]. The principle of the method is described below.

Let us consider that, in fact, the reference trajectory depends on a set of time-varying twice-differentiable parameters p: $\boldsymbol{q}_\mathrm{d} = \boldsymbol{q}_\mathrm{d}[p(t)]$. Various characterizations of the trajectories may appear in p: step length, maximal height of the heel trajectory, time scaling, etc. These parameters are reflected, for example, in the coefficients of the splines that define the trajectories. They are set to a nominal value p^* corresponding to the desired motion. However, since they are supposed to evolve when needed, it is necessary to set their dynamics of return to p^*, through a linear second-order behavior $\ddot{p}_\mathrm{d} = f(p, \dot{p}, p^*)$. Now, it can be shown that it is possible to gather the dynamics, including a PD control scheme like (16.10), the unilaterality of contacts, the requirements of nonsliding and no take-off, and the bounds on actuators, all described in Sect. 16.3.2 and summarized in (16.8), into a single vector inequality of the form

$$\boldsymbol{A}(\boldsymbol{q}, \dot{\boldsymbol{q}}, p, \dot{p}, \ddot{p}) \leq 0\,. \tag{16.11}$$

The problem is now solved by finding at each time through an adequate optimization method (such as FSQP (feasible sequential quadratic programming), originally developed at ISR (Institute of Systems Research), University of Maryland) the parameter acceleration $\ddot{p}$ that minimizes $\|\ddot{p}_d - \ddot{p}\|^2$ while ensuring that (16.11) is satisfied. This approach is, for example, able to compensate for disturbances such as external forces applied to the body, since they are reflected at the internal-state level, and are therefore accounted for through the respect of the inequality (16.11). It has been shown [16.26] that it is possible to increase the range of acceptable disturbances by a factor ten using this method, compared to nonadaptive approaches. Furthermore, the use of exteroceptive sensors such as distance, proximity, and vision is allowed as soon as they directly generate a modification of the parameters, for example, in order to climb a stair or avoid an obstacle.

Online Optimization

The ultimate way to adapt the motion of the robot in real time is to even avoid using any type of precomputed trajectories. This requires that both the desired motion and the related control can be computed online. In the most general case, one can even imagine that these two steps could be fused into a single approach. Besides, thanks to the exponential growth of available embedded computing power, it is now possible to envision the computation of accurate dynamical models and/or the use of complex optimization techniques in real time. This is why we propose to end this part of the chapter with the description of promising optimization-based methods that avoid the explicit synthesis of analytical trajectories.

Model Predictive Control (MPC). The idea is to start from well-known *model predictive control (MPC)* techniques based on the following principle. Let us assume that a dynamical model of the system that is good enough for synthesizing a control scheme is available. Then, the following operations are achieved at each sampling time:

1. measurement of the actual state
2. computation of the control that optimizes a given state-dependent cost function on a finite horizon, starting from the current discrete time
3. application of the control input at the first time index only
4. return to step 1

A main drawback of the standard approach is that the available theoretical results of stability are presently

limited to the linear case or to very particular classes of nonlinear systems. For example, the nonlinear model predictive control (NMPC) presents stability properties under certain assumptions. Moreover, it has some ability to handle constraints, which makes it well suited to the problem of walking pattern synthesis and control of a biped robot subject to unilateral constraints or disturbances due to an unstructured environment. A complete overview of theoretical and practical results concerning the MPC or the NMPC can be found in [16.27]. However, it can be seen from these papers that applying such algorithms is not straightforward when dealing with highly dynamical systems such as robots.

Trajectory-Free NMPC. Following the idea of the parameter adaptation method presented earlier based on the real-time minimization of a cost function through an SQP (sequential quadratic programming) method, an alternative approach consists of solving at every time point a constrained optimization problem with a moving horizon [16.28]. A set of constraints is imposed in order both to ensure the feasibility of walking and to satisfy the user's requirements. Defining these constraints is then the only way which is used to express all the issues involved in the motion of the robot.

As an example of such specifications, let us consider the swing phase in normal steady-state walking. The *inequality* constraints belong to two distinct subsets.

1. Intrinsic constraints related to safety issues:
   - respecting physical limits: the admissible control torques belong to a given set, which may depend on the instantaneous joint velocities; the range of angular joint positions is bounded;
   - ensuring stability: all along the swing phase, the normal contact forces at the support foot are strictly greater than given positive values; the absolute values of the tangential forces are less than given thresholds that depend on the friction parameters.
2. The constraints associated with the gait specification:
   - achieving forward progression: the horizontal velocity of the ankle of the swing leg belongs to a given positive interval; the horizontal position of the pelvis stays inside the position of the toes of the support foot and the horizontal position of the heel of the swinging foot;
   - controlling the posture: the angle expressing the trunk bending is positive and bounded; the angle between the sole of the swing foot and the ground is fixed; the height of the pelvis is low-bounded;
   - ensuring foot clearance: the altitude of the ankle is constrained to stay inside a given area (for example, specified by two polynomial functions of its horizontal position). These functions are a way of avoiding obstacles or climbing stairs.

All these constraints can be gathered in the single vector inequality $g(.) \leq 0$. The *equality* constraints are mainly:

- the dynamics itself (16.6) instanced for the swing phase
- the initial conditions on the state: at time t_{k+1}, they are the final state at time t_k

Therefore the method consists of optimizing, from the inputs (control, state, contact forces, etc.), the anticipated future behavior of the system, subject to the constraints above, using an internal model over a finite sliding time horizon, which is the prediction horizon. Since the problem is finally termed open-loop constrained optimization, solved at each sampling time, the last step is to define an objective function to minimize. Usually, such a cost function includes a term linked to the final state over the prediction horizon and a quadratic expression reflecting some energetic considerations.

The solution of the optimization algorithm is a sequence of N_c control inputs over the prediction horizon N_p. Only the first input is applied to the system and the procedure starts again. It should be noted that the feedback effect, which should be included in any real-time control, appears through the use of *actual* current values of the state in the optimization. Furthermore, the adaptation of the motion in order to react to unexpected events can be performed by modifying online the set of equality and inequality constraints.

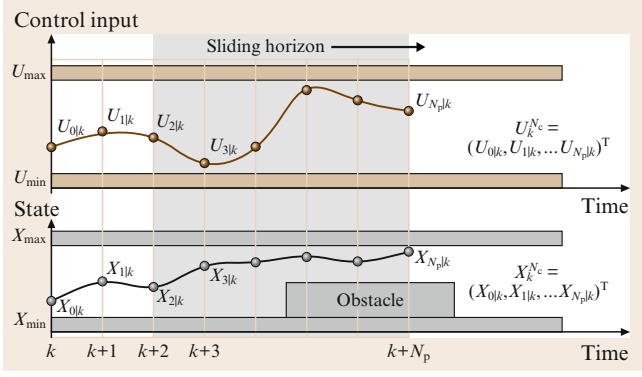

Fig. 16.6 NMPC principles

Let us consider Fig. 16.6, for example. Here, the state $X_{i|k}$ is the prediction of the heel altitude at time $k+i$, computed from the current time k. Then the detection of an obstacle leads to modification of the polynomial that is the lower limit of the trajectory of X. The prediction horizon finally allows one to anticipate the dynamical behavior of the system, which ensures that the foot safely crosses over the obstacle.

This method is known as trajectory-free nonlinear model predictive control and is describe in detail in [16.28]. An extension of the predictive control method to the case of ZMP-based control is presented in [16.29].

16.4 Biped Robots in the ZMP Scheme

The zero-moment point (ZMP) might be one of the most famous technical terms born in robotics community. Figure 16.7 shows two important figures in the scene of ZMP-based biped walking. Figure 16.7a is WL-10RD, developed by Takanishi and Kato. This is the first ZMP-based robot, which successfully realized dynamic biped walking in 1985 [16.30]. It is a 12-degree-of-freedom (DOF) biped, 1.43 m high and weighing 84.5 kg, and driven by hydraulic actuators.

Figure 16.7b is ASIMO, a 26-DOF humanoid robot developed by Honda Motor Co. in 2000 [16.31]. This is one of the most famous robots in public culture, and at the same time, its superior performance of biped locomotion (walking and running) is well acknowledged by specialists. According to the published papers and patents, ZMP takes an important role in the walking control of ASIMO.

In this section, we describe the basic definition, the calculation, and the usage of ZMP.

a) WL-10RD (1985) **b)** ASIMO (2000)

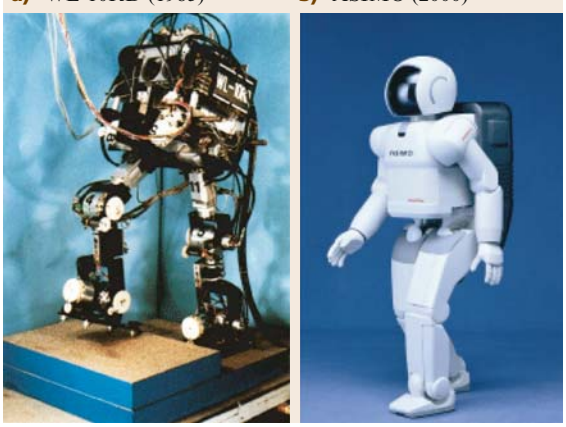

Fig. 16.7a,b Biped robots controlled in the ZMP scheme [16.30, 31]

16.4.1 Mechanisms

Figure 16.8 shows recently developed biped robots controlled by the ZMP scheme. Figure 16.8a is Johnnie, developed by *Gienger* et al. in 2001 [16.32]. It is a 1.80 m-high 17-DOF humanoid weighing 40 kg, driven by direct-current (DC) servo motors with harmonic drive gears and ball screws. Figure 16.8b is HRP-2L, which was developed by *Kaneko* et al. [16.33]. It is a 1.41 m-high 12-DOF biped weighing 58.2 kg, driven by DC servo motors with harmonic drive reduction gears. Figure 16.8c is WL-16R, developed by *Takanishi* et al. [16.34] as a *walking chair* that can carry a human weighing up to 94 kg. It is a 1.29 m-high 12-DOF biped weighing 55 kg with Stewart-platform-type legs driven by electric linear actuators. Figure 16.8d is HUBO, developed by *Oh* et al. [16.35]. It is a 1.25 m-high 41-DOF humanoid robot weighing 55 kg.

Although these robots have different leg mechanism and outlook, they share some common features:

1. there are at least six fully actuated joints for each leg,
2. the joints are position controlled,
3. the feet are equipped with force sensors, which are used to measure the ZMP.

As we will see in the following subsections, these are the fundamental requirements for ZMP-based walking robots.

16.4.2 Zero-Moment Point (ZMP)

The term *zero-moment point (ZMP)* was coined by *Vukobratović* and *Stepanenko* in 1972. They said [16.36]:

> *In Fig. 16.9 an example of force distribution across the foot is given. As the load has the same sign all over the surface, it can be reduced to the resultant force R, the point of attack of which will be*

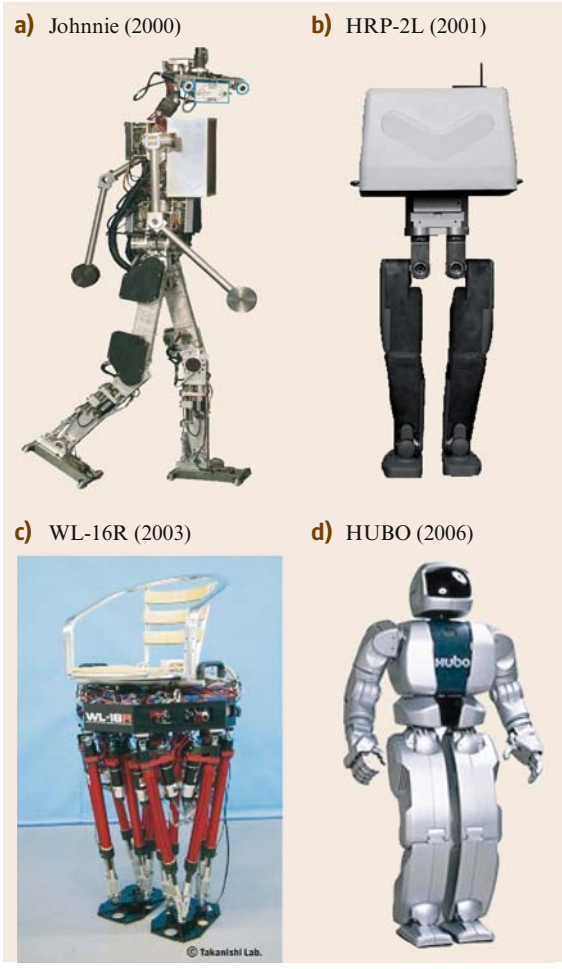

Fig. 16.8a–d Biped robots controlled in the ZMP scheme [16.32–35]

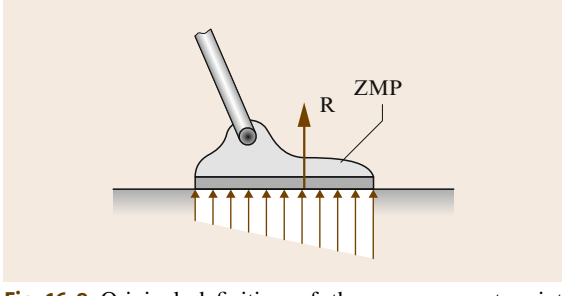

Fig. 16.9 Original definition of the zero-moment point (ZMP) [16.36]

in the boundaries of the foot. Let the point on the surface of the foot, where the resultant R passed, be denoted as the zero-moment point, or ZMP in short.

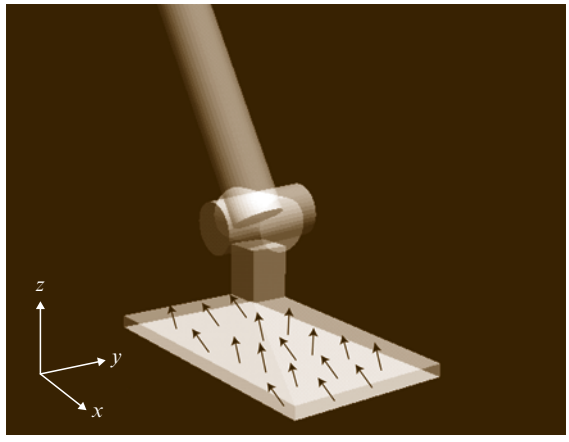

Fig. 16.10 Floor reaction force in three dimensions

We can see that the ZMP is defined as a center of pressure (CoP) of the floor reaction force.

For the further discussion, let us discuss detailed floor reaction force in three dimensions, as shown in Fig. 16.10.

Suppose that the floor reaction force is acting on a finite number of contact points $\boldsymbol{p}_i (i = 1, \ldots, N)$ and that each force vector is of the form

$$\boldsymbol{f}_i := [f_{ix}\, f_{iy}\, f_{iz}]^\top ,$$

where f_{ix}, f_{iy}, and f_{iz} are the force components in the x, y, and z directions in the coordinate system fixed to the ground, respectively. The ZMP can be calculated as

$$\boldsymbol{p} := \frac{\sum_{i=1}^{N} \boldsymbol{p}_i f_{iz}}{\sum_{i=1}^{N} f_{iz}} . \tag{16.12}$$

It can also be written as

$$\boldsymbol{p} = \sum_{i=1}^{N} \alpha_i \boldsymbol{p}_i , \tag{16.13}$$

$$\alpha_i := f_{iz} / f_z , \tag{16.14}$$

$$f_z := \sum_{i=1}^{N} f_{iz} . \tag{16.15}$$

Since an ordinary walking robot cannot generate adhesive force on its soles,

$$f_{iz} \geq 0 \qquad (i = 1, \ldots, N) . \tag{16.16}$$

Then we can say,

$$\begin{cases} \alpha_j \geq 0 \qquad (i = 1, \ldots, N) \,, \\ \sum_{i=1}^{N} \alpha_i = 1 \,. \end{cases} \tag{16.17}$$

The points that satisfy (16.13) and (16.17) form the *support polygon*, the convex hull of the contacting point. Thus, we can conclude that the ZMP always exists in the support polygon. In other words, *the ZMP never leaves the support polygon* as the result of the unilateral constraint on the floor reaction force.

Now let us calculate the torque around the ZMP:

$$\boldsymbol{\tau} = \sum_{i=1}^{N} (\boldsymbol{p}_i - \boldsymbol{p}) \times \boldsymbol{f}_i \,. \tag{16.18}$$

This equation can be rewritten in terms of vector components as

$$\tau_x = \sum_{i=1}^{N} (p_{iy} - p_y) f_{iz} - \sum_{i=1}^{N} (p_{iz} - p_z) f_{iy} \,, \tag{16.19}$$

$$\tau_y = \sum_{i=1}^{N} (p_{iz} - p_z) f_{ix} - \sum_{i=1}^{N} (p_{ix} - p_x) f_{iz} \,, \tag{16.20}$$

$$\tau_z = \sum_{i=1}^{N} (p_{ix} - p_x) f_{iy} - \sum_{i=1}^{N} (p_{iy} - p_y) f_{ix} \,, \tag{16.21}$$

where p_{ix}, p_{iy}, p_{iz} are the components of the position vector $\boldsymbol{p}_i$ and p_x, p_y, and p_z are the components of the ZMP.

When the floor is horizontal, we have $p_{iz} = p_z$ for all i, thus, the second term of (16.19) and the first term of (16.20) become zero. Moreover, by substituting (16.12) into (16.19) and (16.20), we obtain

$$\tau_x = \tau_y = 0 \,. \tag{16.22}$$

This is the reason why $\boldsymbol{p}$ was named as *zero-moment* point. Nevertheless, one must note that the frictional force creates a nonzero vertical moment (16.21) in the general case.

$$\tau_z \neq 0 \,. \tag{16.23}$$

16.4.3 Computed ZMP: ZMP Calculated from Robot Motion

With given robot dynamics and motion, we can calculate or predict the resulting ZMP by using Newton's law. To distinguish this from the original ZMP defined in the former subsection, we will use the term *computed ZMP* as in the paper of *Vukobratović* et al. [16.3]

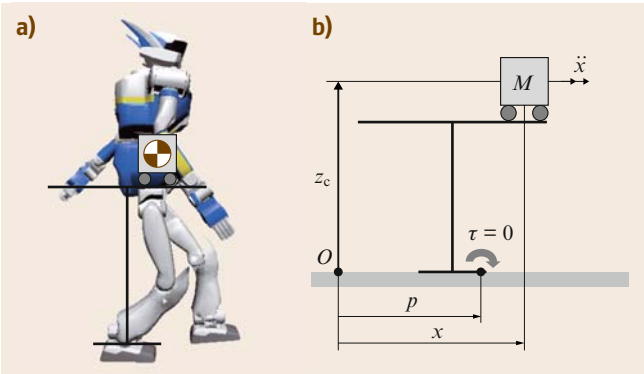

Fig. 16.11a,b Cart–table model [16.37]

Simple Case

Let us start with an extremely simple mechanism. Figure 16.11a illustrates a walking robot and its simplified model, which consists of a running cart on a massless table. The cart has mass M and its position is (x, z_c) corresponds to the center of mass of the robot (Fig. 16.11b). Also, the table is assumed to have the same support polygon as the robot.

In this case, the torque τ around the point p is given by

$$\boldsymbol{\tau} = -Mg(x - p) + M\ddot{x} z_c \,, \tag{16.24}$$

where g is the acceleration due to gravity. Using the zero-moment condition of $\boldsymbol{\tau} = 0$, the computed ZMP of this cart–table model is obtained as

$$p = x - \frac{z_c}{g} \ddot{x} \,. \tag{16.25}$$

From this equation, we can observe two fundamental facts about the computed ZMP.

1. When the acceleration of the cart is zero, the ZMP corresponds to the projection of the CoM: $p = x$.
2. The computed ZMP is not bounded by the support polygon. In fact, we can easily determine x and $\ddot{x}$ to give any specified value of p.

The second fact is explained in Fig. 16.12a. When the cart acceleration is too large, the computed ZMP goes outside of the support polygon. This happens since (16.25) does not consider the support polygon and the unilateral constraint (16.16). In other words, (16.25) assumes that the foot is glued to the floor. If the unilateral constraint is properly considered, we have the state of

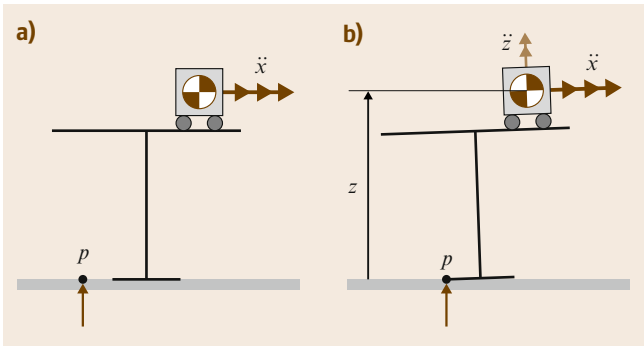

Fig. 16.12a,b Computed ZMP (a) fictitious case (b) correct result

Fig. 16.12b. Since the table is no longer upright, the computed ZMP must be calculated by

$$p = x - \frac{z}{g+\ddot{z}}\ddot{x}\,, \tag{16.26}$$

which gives the computed ZMP on the edge of support polygon.

In much of the literature, states like Fig. 16.12b are not explicitly discussed, but the computed ZMP is allowed to leave the support polygon under the implicit assumption of the glued foot on the floor. In this case, a computed ZMP outside of the support polygon implies that the robot might not maintain its feet in full contact with the ground and that the walking motion will not be performed as planned.

When the computed ZMP is inside the support polygon, it guarantees the full foot-ground contact under the unilateral constraint, while it tells us nothing about *stability* in the context of control theory.

Computed ZMP for Full 3-D Dynamics

We will show a method to calculate the computed ZMP of a robot that consists of N rigid-body links in three dimensions. As in the preceding treatment, we assume that the all kinematic information (the position of the CoM, link orientation, link velocity, etc.) have already been calculated by forward kinematics. In this subsection, the link postures and their angular velocities are represented in the ground-fixed coordinate system.

First we calculate the total mass M and the center of mass of the whole robot $\boldsymbol{c}$ by

$$M = \sum_{j=1}^{N} m_j\,, \tag{16.27}$$

$$\boldsymbol{c} = \sum_{j=1}^{N} m_j \boldsymbol{c}_j / M\,, \tag{16.28}$$

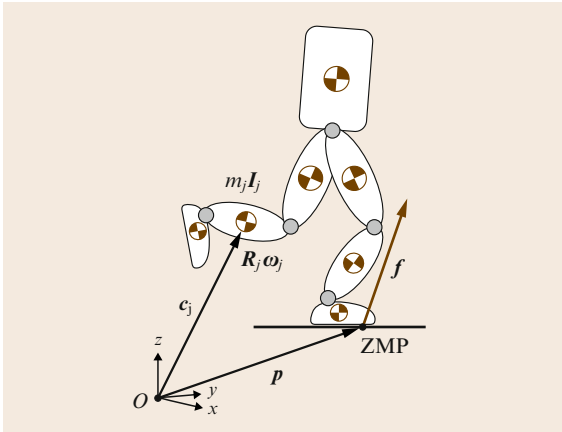

Fig. 16.13 Robot model and ZMP in three dimensions

where m_j and $\boldsymbol{c}_j$ are the mass and the CoM of the j-th link, respectively.

The total linear momentum $\mathcal{P}$ is given as

$$\mathcal{P} = \sum_{j=1}^{N} m_j \dot{\boldsymbol{c}}_j\,. \tag{16.29}$$

Then the total angular momentum $\mathcal{L}$ with respect to the origin is

$$\mathcal{L} = \sum_{j=1}^{N} \left[\boldsymbol{c}_j \times (m_j \dot{\boldsymbol{c}}_j) + \boldsymbol{R}_j \boldsymbol{I}_j \boldsymbol{R}_j^{\top} \boldsymbol{\omega}_j\right], \tag{16.30}$$

where $\boldsymbol{R}_j$, $\boldsymbol{I}_j$, and $\boldsymbol{\omega}_j$ are the 3×3 rotation matrix, inertia tensor, and angular velocity of the j-th link, respectively. $\boldsymbol{R}_j \boldsymbol{I}_j \boldsymbol{R}_j^{\top}$ gives the inertia tensor in the ground-fixed frame.

Applied with the external force $\boldsymbol{f}$ and external moment $\boldsymbol{\tau}$, the change of linear and angular momenta are described by Newton and Euler's law:

$$\boldsymbol{f} = \dot{\mathcal{P}} - M\boldsymbol{g}\,, \tag{16.31}$$

$$\boldsymbol{\tau} = \dot{\mathcal{L}} - \boldsymbol{c} \times M\boldsymbol{g}\,, \tag{16.32}$$

where $\boldsymbol{g} := [0\,0\,-g]^{\top}$ is the vector of acceleration due to gravity.

Suppose that the external force is acting on the ZMP located at $\boldsymbol{p}$.

$$\boldsymbol{\tau} = \boldsymbol{p} \times \boldsymbol{f} + \boldsymbol{\tau}_{\mathrm{ZMP}}\,, \tag{16.33}$$

where $\boldsymbol{\tau}_{\mathrm{ZMP}}$ is the moment at the ZMP, whose first and second components are zero.

Substituting (16.31) and (16.32) into (16.33) we obtain

$$\boldsymbol{\tau}_{\mathrm{ZMP}} = \dot{\mathcal{L}} - \boldsymbol{c} \times M\boldsymbol{g} + (\dot{\mathcal{P}} - M\boldsymbol{g}) \times \boldsymbol{p}\,. \tag{16.34}$$

The first and the second raws of this equation are

$$\tau_{\mathrm{ZMP},x} = \dot{\mathcal{L}}_x + Mgy + \dot{\mathcal{P}}_y p_z - (\dot{\mathcal{P}}_z + Mg)p_y \,, \tag{16.35}$$

$$\tau_{\mathrm{ZMP},y} = \dot{\mathcal{L}}_y - Mgx - \dot{\mathcal{P}}_x p_z + (\dot{\mathcal{P}}_z + Mg)p_x \,, \tag{16.36}$$

where we use the notations

$$\begin{aligned}
\boldsymbol{\tau}_{\mathrm{ZMP}} &=: [\tau_{\mathrm{ZMP},x}\, \tau_{\mathrm{ZMP},y}\, \tau_{\mathrm{ZMP},z}]^\top \,, \\
\mathcal{P} &=: [\mathcal{P}_x \mathcal{P}_y \mathcal{P}_z]^\top \,, \\
\mathcal{L} &=: [\mathcal{L}_x \mathcal{L}_y \mathcal{L}_z]^\top \,, \\
\boldsymbol{c} &=: [x\ y\ z]^\top \,.
\end{aligned}$$

The zero-moment point is calculated from (16.35) and (16.36) using $\tau_{\mathrm{ZMP},x} = \tau_{\mathrm{ZMP},y} = 0$

$$p_x = \frac{Mgx + p_z\dot{\mathcal{P}}_x - \dot{\mathcal{L}}_y}{Mg + \dot{\mathcal{P}}_z} \,, \tag{16.37}$$

$$p_y = \frac{Mgy + p_z\dot{\mathcal{P}}_y + \dot{\mathcal{L}}_x}{Mg + \dot{\mathcal{P}}_z} \,, \tag{16.38}$$

where p_z is the height of the floor.

When the robot remains stationary, we have the ZMP as the projection of the CoM:

$$p_x = x \,, \tag{16.39}$$

$$p_y = y \,. \tag{16.40}$$

Note that ZMP can also be calculated from the motion equation in Lagrangian form. See Sect. 16.3.2 for more details.

16.4.4 ZMP-Based Walking Pattern Generation

Prescribing Foot and ZMP Trajectories

In the original work, a model with a compensating mechanism was assumed to realize the prescribed ZMP pattern [16.36]. Figure 16.14a illustrates an example model, which uses predetermined leg trajectories while ZMP is controlled by using the compensating mass. This concept was realized by the WL-12 robot developed by *Takanishi* and *Kato* (Fig. 16.14b) [16.38].

In modern implementations, the body motion is used to realize prescribed ZMP trajectories, as shown in Fig. 16.15. Instead of the leg joint trajectories, the foot trajectories are prescribed. The leg motion is determined by inverse kinematics from the body and the feet trajectories.

Figure 16.16 shows an example ZMP trajectory for two forward steps. First, the time profile of the support polygon is determined from the foot trajectory as the gray band. Its width is determined from the foot geometry and the step length and changes at every touchdown (td) and lift-off (lo). Then the ZMP trajectory (bold line) is determined so that it runs within the support polygon. Note that we can design any ZMP trajectories as long as it remains inside of the support polygon with a certain stability margin.

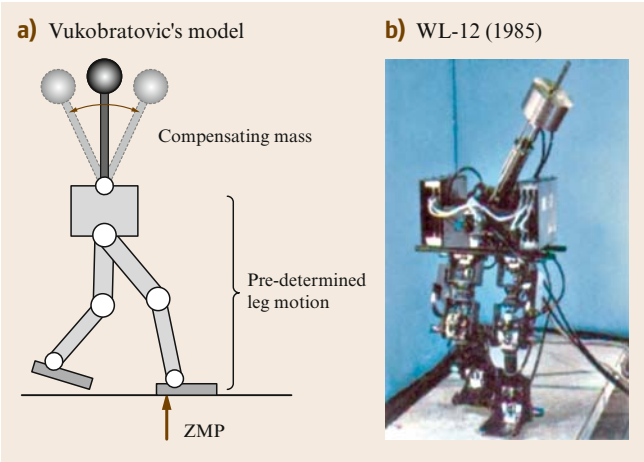

Fig. 16.14a,b Biped robots with compensating mass [16.38]

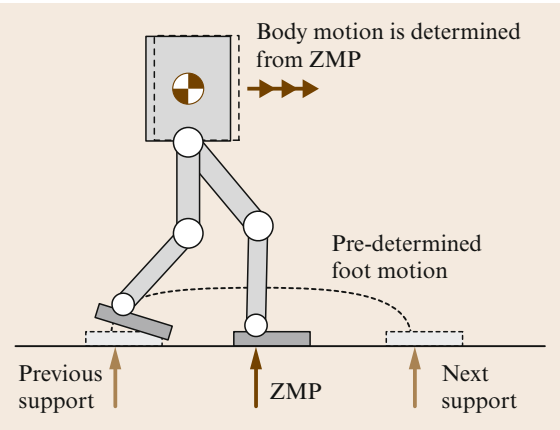

Fig. 16.15 Modern implementation of the ZMP scheme

Pattern Generation for the Desired ZMP

Let us define a function *ZMP*() that gives a calculated ZMP for the given robot motion.

$$\begin{pmatrix} p_x \\ p_y \end{pmatrix} = ZMP(\boldsymbol{q}, \dot{\boldsymbol{q}}, \ddot{\boldsymbol{q}}), \tag{16.41}$$

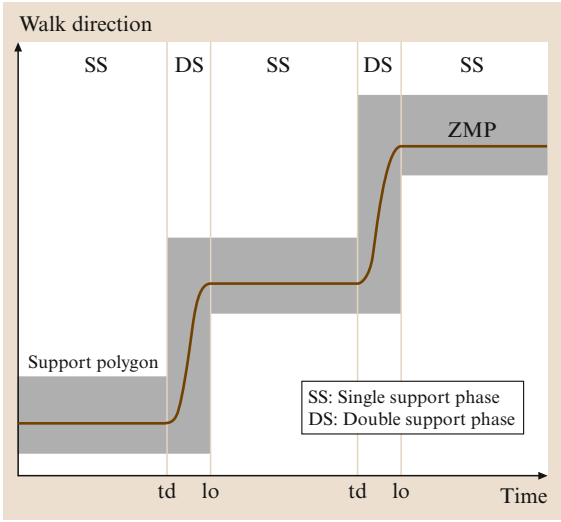

Fig. 16.16 Support polygon and prescribed ZMP trajectory. td: touchdown; lo: lift-off

where $\boldsymbol{q}$, $\dot{\boldsymbol{q}}$, and $\ddot{\boldsymbol{q}}$ are the vectors of joint position, velocity, and acceleration, respectively. ZMP-based walking pattern generation is to determine the feasible $\boldsymbol{q}(t)$ that satisfies given desired ZMP $p_x^{\mathrm{d}}(t)$, $p_y^{\mathrm{d}}(t)$. It should be noted that:

1. As the premise of this method, the robot must be fully actuated and position controlled. Basically, underactuated or torque-controlled robots do not fit in this scheme.
2. When the dimension of $\boldsymbol{q}$ is larger than three, extra constraints must be introduced to solve the redundancy. For example, constraints of constant body height and upright posture are frequently used.
3. Even under the proper constraints, (16.41) have infinite numbers of solutions because the initial condition $\boldsymbol{q}(0)$ is left free. This degree of freedom is used to avoid the divergence of the joint trajectories.
4. In practice, we do not need an exact control of ZMP: $p_x(t) = p_x^{\mathrm{d}}(t)$, $p_y(t) = p_y^{\mathrm{d}}(t)$. Nevertheless, it is preferred to minimize the sum of ZMP error during the walking motion.

Several practical methods have been proposed. *Takanishi* et al. proposed to solve this problem by using Fourier transformation [16.39]. By applying the fast Fourier transformation (FFT) to the ZMP reference, the ZMP equations can be solved in the frequency domain, then the inverse FFT returns the resulted CoM trajectory to the time domain. *Kagami* et al. proposed a method to solve this problem in the discrete time domain [16.40]. They showed that the ZMP equation can be discretized as a trinomial expression, and that it can be solved efficiently by an algorithm of $O(N)$ for given reference data of size N.

Another practical method was described by *Huang* et al. [16.41]. *Sugihara* et al. proposed a method that can consider the multibody dynamics of a robot [16.42]. *Nagasaka* et al. proposed an efficient real-time method that is also applicable to running and jumping motion [16.43]. *Harada* et al. proposed another efficient real-time method that can be used when pushing an object during walking [16.44].

Pattern Generation Using Preview Controller

In this subsection, we will describe the method proposed by *Kajita* et al. [16.37]. Its stability and possible expansions are well discussed by *Wieber* [16.29].

For the simplicity, let us use the cart–table model of Fig. 16.11 again, but this time, we take the jerk of the cart as the system input u,

$$\dddot{x} = u \,. \tag{16.42}$$

In this way, the ZMP equation (16.25) can be translated into a strictly proper dynamical system as

$$\frac{\mathrm{d}}{\mathrm{d}t}\begin{pmatrix} x \\ \dot{x} \\ \ddot{x} \end{pmatrix} = \begin{pmatrix} 0 & 1 & 0 \\ 0 & 0 & 1 \\ 0 & 0 & 0 \end{pmatrix}\begin{pmatrix} x \\ \dot{x} \\ \ddot{x} \end{pmatrix} + \begin{pmatrix} 0 \\ 0 \\ 1 \end{pmatrix} u \,, \tag{16.43}$$

$$p = \begin{pmatrix} 1 & 0 & -z_{\mathrm{c}}/g \end{pmatrix}\begin{pmatrix} x \\ \dot{x} \\ \ddot{x} \end{pmatrix} .$$

For this system, we can design a digital controller that lets the system output follow the reference input as

$$u(k) = -G_i \sum_{i=0}^{k} e(i) - G_x \boldsymbol{x}(k) \,, \tag{16.44}$$

$$e(i) := p(i) - p^d(i) \,,$$

where G_i is the gain for the ZMP tracking error, G_x is the state feedback gain, and $\boldsymbol{x} := [x\dot{x}\ddot{x}]^{\top}$. The value at the k-th sample time is indicated by appending (k). The block diagram of the feedback system is shown in Fig. 16.17.

Although we can guarantee the stability of this system by LQ (linear quadratic) feedback gains, the controller of (16.44) cannot realize sufficient ZMP tracking due to the phase delay. To solve this problem, we must

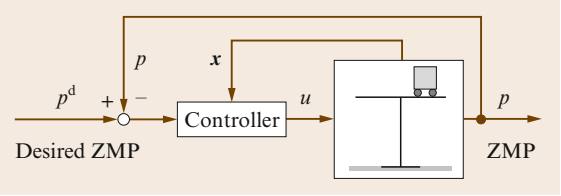

Fig. 16.17 ZMP tracking control

use the following controller:

$$u(k) = -G_i \sum_{i=0}^{k} e(i) - G_x \boldsymbol{x}(k) - \sum_{j=1}^{N_L} G_p(j) p^d(k+j) \tag{16.45}$$

The third term is new and contains the ZMP reference up to N_L samples future. Since this controller uses future information, it is called a *preview controller* [16.45,46]. The gain $G_p(j)$ is called the preview gain and Fig. 16.18 shows its profile towards the future. We can observe that the magnitude of the preview gain quickly diminishes, thus the ZMP reference in the far future can be neglected.

Figure 16.19 shows an example of a walking pattern generated by using a preview controller. The upper graph shows the sagittal motion along the x-axis and the lower graph shows the lateral motion along the y-axis. We can see that a smooth trajectory of the CoM (dashed line) is generated and that the resulting ZMP (bold line) follows the reference (thin line) with good accuracy.

16.4.5 ZMP-Based Walking Control

If we have an ideal mechanism on a perfect flat floor, we can expect that a robot walks just by a playback of prescribed joint trajectory. Since this is not the case in general, we need feedback control to modify the reference trajectory using sensor information, as shown in Fig. 16.20. Such stabilizers are discussed in [16.25,47–50].

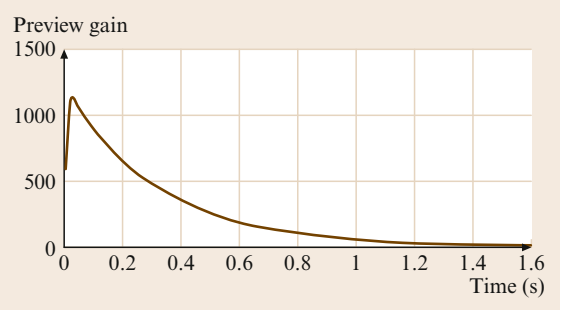

Fig. 16.18 Preview controller gain G_p (sample time $T = 5$ ms, $z_c = 0.814$ m, $Q_e = 1.0$, $Q_x = 0$, $R = 1.0 \times 10^{-6}$)

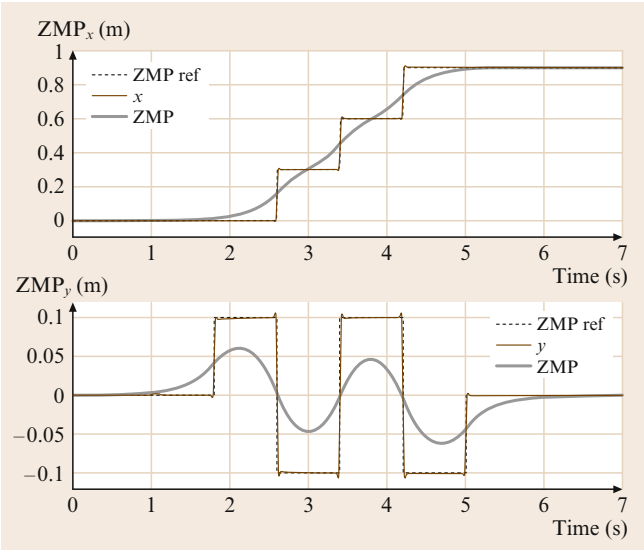

Fig. 16.19 Body trajectory obtained by preview control; previewing period $TN_L = 1.6$ s

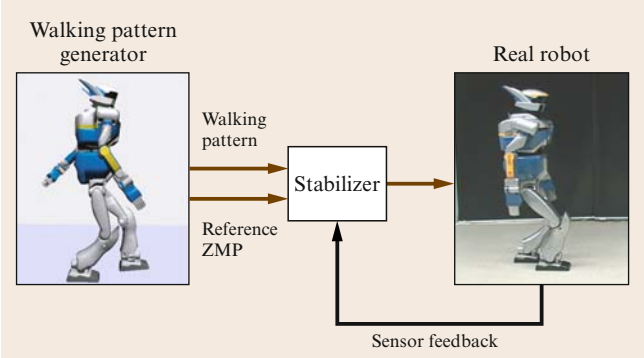

Fig. 16.20 Pattern generator and stabilizer

16.4.6 Expansion of the ZMP Concept

We can predict a robot fall when the CoM projection is observed outside of the support polygon. However, we cannot use the ZMP by this way, since the ZMP never leaves the support polygon of a real biped robot. When the ZMP is on the edge of the support polygon, all we can say is that *the robot can fall*, since it is merely a necessary condition of falling. As an alterna-

tive of ZMP, *Goswami* proposed a foot-rotating indicator (FRI) [16.51]. FRI is a ZMP calculated by omitting the acceleration of the supporting foot and is a measurable value of real robots that may leave the support polygon. When am FRI is outside of the support polygon, this indicates a support foot acceleration, which breaks a foot–floor contact.

Another problem is that the ZMP is defined only on the flat plane. *Sardain* and *Bessonnet* discussed a general ZMP calculation including a double support phase on uneven terrain [16.52].

Saida et al. proposed a feasible solution of wrench (FSW) as a new criterion for a legged robot on uneven terrain [16.53].

Hirukawa et al. also proposed a universal stability criterion that can treat a general geometry of foot–ground contact and unidirectional force constraints [16.54].

16.5 Multilegged Robots

This section treats robots that have more than three legs.

16.5.1 Analysis of Static Gait

Compared with bipeds, multilegged robots have a wider choice of foot placing to maintain static balance. From this reason, many research works have concentrated on gait planning for statically stable walking rather than treating dynamic stability. In this subsection, we will introduce those important results by following *McGhee* [16.55] and *Song* and *Waldron* [16.56].

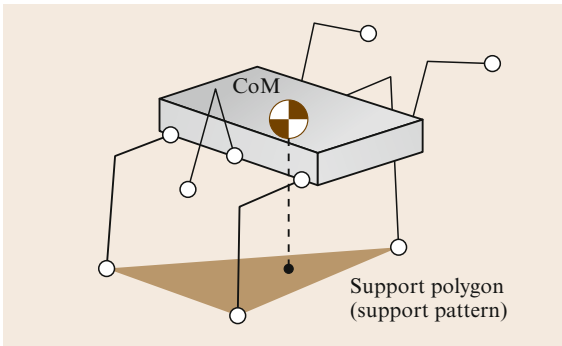

Fig. 16.21 Support polygon (support pattern) of a multilegged robot

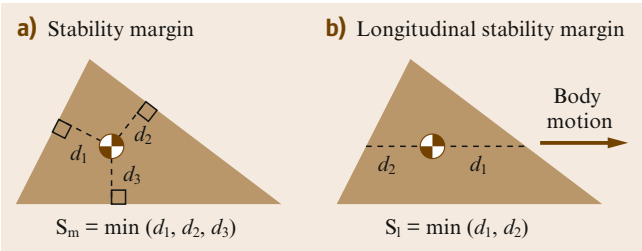

Fig. 16.22a,b Definition of stability margins

Stability Margins

In multilegged robot research, the term *support pattern* is frequently used for support polygon [16.55–57]. By neglecting the inertial effects caused by body and leg acceleration, we can guarantee that the robot maintains balance if the projection of the CoM falls inside the support pattern, as shown in Fig. 16.21.

For a given configuration of a walking robot, the *stability margin* S_m is defined as the minimum distance of the vertical projection of CoM to the boundaries of the support pattern in the horizontal plane, as illustrated in Fig. 16.22a. In addition, an alternative index was proposed to obtain the optimal gait analytically. That is the *longitudinal stability margin* S_l, which is defined as the minimum distance from the vertical projection of the CoM to the support pattern boundaries along the line parallel to the body motion.

Quadruped Creeping Gait and Crawl Gait

From the front to the rear of a $2n$-legged robot or animal, let us index the left legs and the right legs by odd numbers $1, 3, \ldots, 2n-1$ and even numbers $2, 4, \ldots, 2n$, respectively. Following this rule, the legs of a quadruped robot are numbered as in Fig. 16.23.

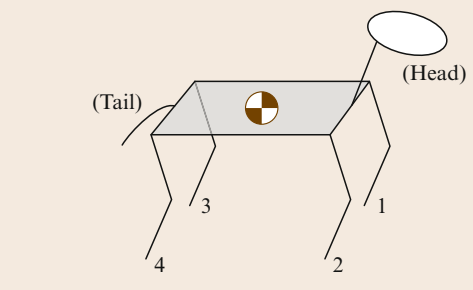

Fig. 16.23 Leg labeling of quadruped robot

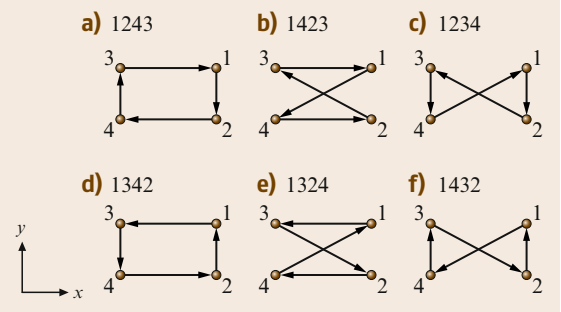

Fig. 16.24a–f Quadruped creeping gaits [16.57]

To walk keeping static stability, a quadruped robot must lift and place only one leg at each step. In general, such a pattern is called *creeping gait*. The possible creeping gaits of a quadruped robot can be expressed by a series of leg numbers to show the order of foot placing. Always choosing leg 1 as the first swing leg, we can distinguish $(4-1)! = 6$ different gaits, as shown in Fig. 16.24.

As we will see later, the 1423 creeping gait (Fig. 16.24b) gives the maximum stability for waking along the x-direction, and is called the *crawl gait*. Note that if the walking direction was $-x$, 1324 (Fig. 16.24e) gives the crawl gait. Likewise, 1234 (Fig. 16.24c) and 1432 (Fig. 16.24f) represent the crawl gait in the $-y$ and y directions, respectively.

On the other hand, the 1243 and 1342 creeping gaits (Fig. 16.24a, d) gives medium stability and are suitable for turning.

Gait Diagram

Figure 16.25b is a *gait diagram* to describe the gait sequence of a multilegged robot. The horizontal axis indicates the time normalized by walk cycle time T. The line segment associated with each leg starts from the touchdown and ends at lift-off. Therefore, the length of the line segment indicates the period of the support phase. From this diagram, we can define the *duty factor* β_i and *phase* ϕ_i of leg i as

$$\beta_i = \frac{\text{support period of leg } i}{T}\,, \tag{16.46}$$

$$\phi_i = \frac{\text{touchdown time of leg } i}{T}\,. \tag{16.47}$$

The touchdown time of leg i is measured from the touchdown of leg 1; therefore, we have $\phi_1 = 0$ for any gait.

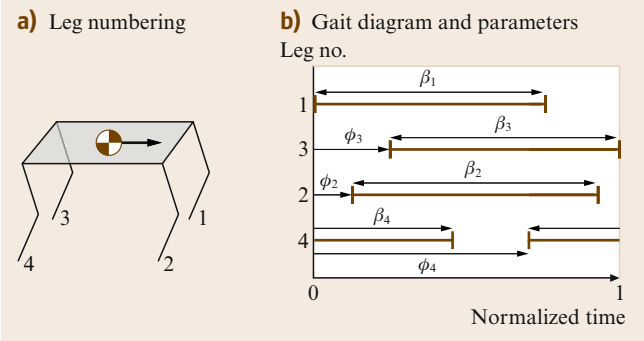

Fig. 16.25a,b Gait diagram and parameters

Wave Gait of Quadrupeds

There exists a special gait which gives maximum longitudinal stability margin for a quadruped robot [16.57]. It is called the *wave gait* defined as

$$\beta_i = \beta, \qquad (i = 1, \ldots, 4)\,, \tag{16.48}$$

$$0.75 \le \beta < 1\,, \tag{16.49}$$

$$\phi_2 = 0.5\,, \tag{16.50}$$

$$\phi_3 = \beta\,, \tag{16.51}$$

$$\phi_4 = \phi_3 - 0.5\,, \tag{16.52}$$

where β is the duty factor of the wave gait. Figure 16.26 shows the gait diagram of a wave gait of $\beta = 0.75$.

If we look at the order of foot placement in Fig. 16.26, it is a crawl gait (1423 creeping gait) shown in Fig. 16.24b. Therefore, a wave gait is the optimal crawl gait.

The most important feature of the wave gait is specified by (16.51). This means that leg 3 touchdowns at the moment of leg 1's lift-off, as indicated by the ellipse (broken line) in Fig. 16.26. Equation (16.49) gives the possible range of duty factor for a statically stable walking. In addition, a wave gait is characterized as *regular* and *symmetric*. A gait is regular when all legs have the same duty factor β, as specified by (16.48). A gait is

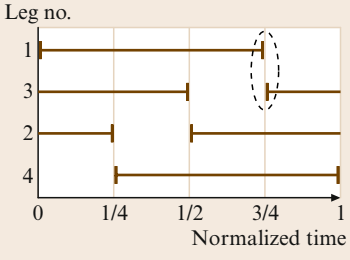

Fig. 16.26 Wave gait of a quadruped robot ($\beta = 0.75$)

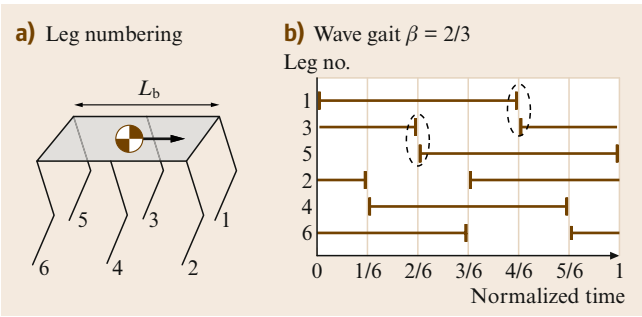

Fig. 16.27a,b Wave gait of a hexapod robot

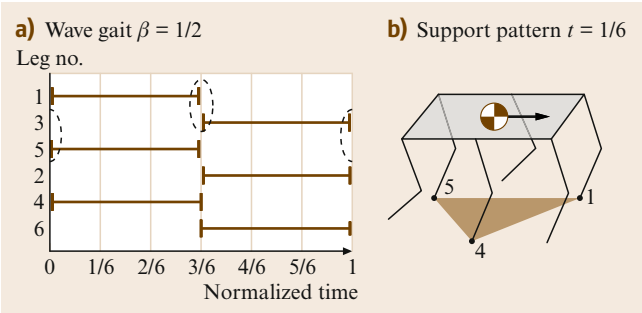

Fig. 16.28a,b Tripod gait of a hexapod robot

symmetric when the right and the left leg of each column has a phase difference of a half-cycle, 0.5 as specified by (16.50) and (16.52).

Wave Gait of 2*n*-Legged Robots

A wave gait of $2n$-legged robots can be defined as a regular and symmetric gait with the following feature.

$$\phi_{2m+1} = F(m\beta), \quad (m = 1, \ldots, n-1), \tag{16.53}$$

$$3/(2n) \le \beta < 1, \tag{16.54}$$

where $F(x)$ gives the fractional part of a real number x. Equation (16.53) is a generalization of (16.51). An example wave gait for hexapod robot is shown in Fig. 16.27. The ellipses (broken line) show the condition (16.53).

Figure 16.28 shows a wave gait with $\beta = 1/2$, which is the most important for hexapod robots. From the constraint (16.54), this is the smallest duty factor for hexapods and thus results in the fastest walking speed. This gait is specially called a *tripod gait* since a robot is supported by the three legs 145 and 236 reciprocally (Fig. 16.28b).

It is known that *the longitudinal gait stability margin of a* $2n$*-legged robot is maximized by wave gaits* [16.56]. Figure 16.29 shows the optimal wave-gait stability margin normalized by body length L_b (Fig. 16.27a) for

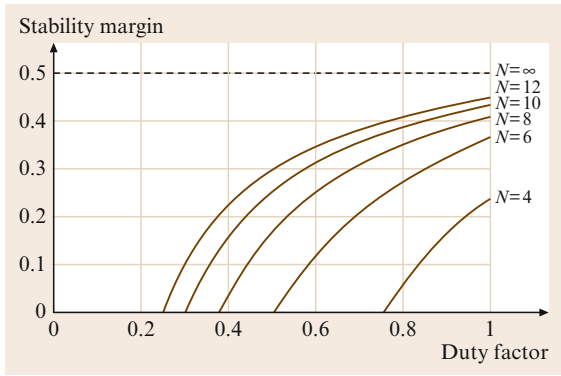

Fig. 16.29 Optimal wave-gait stability margin of N-legged locomotion systems [16.55]

Fig. 16.30 The adaptive suspension vehicle (1986) [16.58]

N-legged robots [16.55]. We can observe that by increasing the number of legs the stability and allowable range of duty factors are improved. The largest improvement is obtained from $N = 4$ to 6 and the gains gradually become small towards $N = \infty$. Since the cost of the hardware goes up in proportion to the number of the legs, this explains the rarity of developed robots with more than ten legs.

16.5.2 Practical Gait Design

Unlike the ideal analysis in previous section, real multi-legged robots are far more complex. In this subsection, we see more practical aspects of gait control by concentrating on a few state-of-the-art examples.

Hexapod: The Adaptive Suspension Vehicle

Figure 16.30 shows one of the most famous hexapods, the adaptive suspension vehicle (ASV) developed by *Waldron* and *McGhee* [16.56, 58]. The ASV is a hy-

Table 16.1 Specifications of the ASV [16.56]

Dimensions:	5.2 m in length
	3.0 m in height
	2.4 m in track width
Degree of freedom	18 DOF (3 DOF × 6)
Weight	2700 kg
Payload	220 kg
Speed	8 km/h
Grade climb ability:	60% gradient
Mobility:	Ditch crossing: 1.8 m
	Vertical step crossing: 1.7 m
	Isolated wall crossing: 1.4 m
	Fording depth: 1.2 m

Table 16.2 Gait used by the ASV [16.56]

Periodic	Wave gait
	Equal phase gait
	Backward wave gait
	Backward equal-phase gait
	Dexterous periodic gait
	Continuous follow-the-leader gait
Nonperiodic	Discontinuous follow-the-leader gait
	Large-obstacle gait
	Precision footing gait
	Free gait

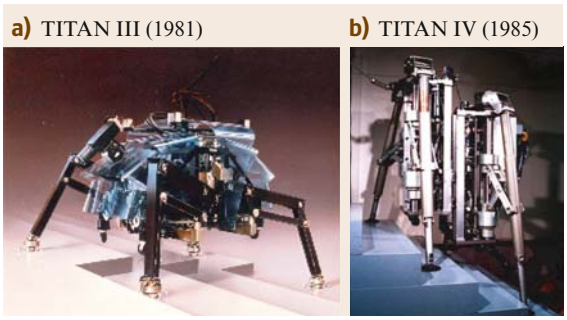

Fig. 16.31a,b The TITAN series [16.59, 60]

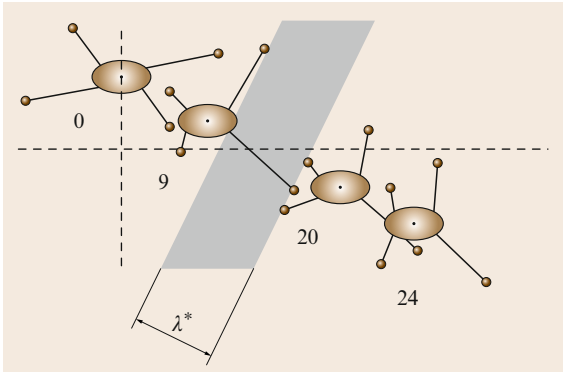

Fig. 16.32 Walking motion over a river [16.61]

draulically driven hexapod robot that can carry a parson over rough terrain. Table 16.1 lists the design specifications and mobility of the ASV at experimentation in natural terrain.

Table 16.2 shows the variety of gaits that was used to control the ASV. We can see that the wave gait appears at the top of list, however, it requires undesirable peak power consumption at certain moments. The *equal-phase gait* was designed to solve this problem. Another interesting gait is the *follow-the-leader* gait in which the middle foot is placed on the footprint made by the front foot, and the rear foot is placed in the footprint of the middle foot. By using this gait, the load on the human operator to specify foot placement when moving over difficult terrain can be drastically reduced. In this manner, each gait listed in Table 16.2 has some advantage depending on the ground adaptivity, power consumption or smoothness of body motion.

Quadruped: TITAN Series

Figure 16.31 shows quadruped robots developed by *Hirose* and his colleagues [16.59, 60]. TITAN III (Fig. 16.31a) has four legs, each 1.2 m long, and weighs 80 kg. Each leg is driven by three DC motors, thus this is a 12-DOF walking robot. On flat ground, TITAN III uses a generalized crawl gait which allows the robot to move omnidirectionally (*crab-walk gait*). When the robot step into a rough terrain it uses *free gait*, which is a nonperiodic gait to search for safe footholds, avoiding obstacles and maintaining static stability. Figure 16.32 shows an example of free gait to walk over a river. Once the robot returns to flat ground, it is controlled to return the crab-walk gait, which is more efficient.

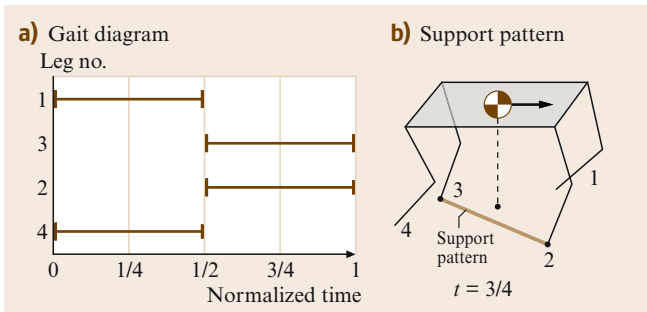

Fig. 16.33a,b Trot gait

TITAN IV (Fig. 16.31b) has a similar configuration to TITAN III, but weighs 160 kg. Since it has much powerful motors, an experiment of dynamic walk was conducted. For a given return speed of the swing leg U, the walking speed with duty factor β is

$$V = \frac{1-\beta}{\beta} U \,. \tag{16.55}$$

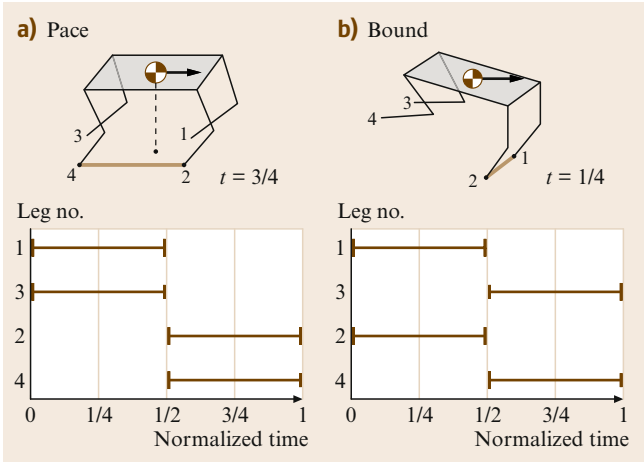

Fig. 16.34a,b Another dynamic gait of quadrupeds

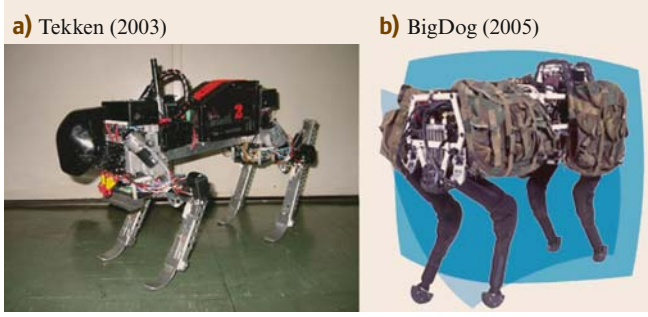

Fig. 16.35a,b Quadruped robots inspired by mammals [16.62, 63]

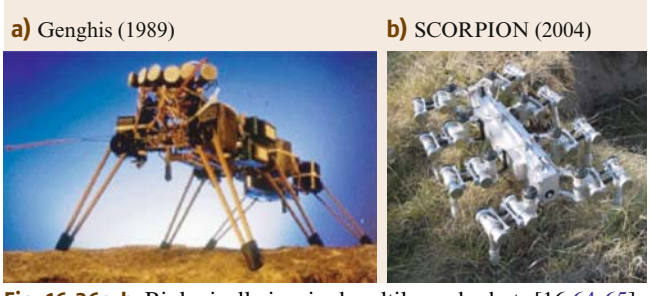

Fig. 16.36a,b Biologically inspired multilegged robots [16.64, 65]

For a statically stable wave gait, the smallest β is 0.75 (Sect. 16.5.1), thus $V = 0.33U$ is the maximum speed. However, by using a duty factor of $\beta = 0.5$, we can achieve $V = U$, three times faster than the maximum speed of static walk. Figure 16.33 shows such a gait. The gait diagram (Fig. 16.33) shows that the robot stands on two legs at all times, which is called the *trot gait*.

As illustrated in Fig. 16.33b, a trot gait is a dynamic walk where the ZMP should be controlled to be inside the support pattern (support polygon) while the projection of the CoM goes outside of it. *Hirose* et al. introduced the body swaying control to meet the ZMP condition and the *expanded trot gait* for a smooth transition from a static gait at slow speed to a dynamic gait at high speed [16.60]. Later, this technique was elaborated for TITAN VI, the successor to TITAN IV [16.66].

16.5.3 Dynamic Quadrupeds Inspired by Mammals

Nature exhibits a variety of implementations of legged locomotion and some of them are much more dynamic than in the analysis and synthesis discussed above. Figure 16.34 shows two dynamic gaits used by mammals [16.67]. Pace is used by camels and bound is used by running dogs, for example.

Raibert showed that trot, pace, and bound can be regarded as biped locomotion by pairing diagonal legs, font–rear legs, and lateral legs, respectively. Using this idea, he demonstrated a hydraulic running quadruped that can trot, pace, and bound [16.5]. Such gaits have also been realized by electrically powered quadrupeds using different control schemes [16.68, 69].

Figure 16.35a shows recently developed mammal-like quadruped robots. Tekken is an electric quadruped robot with a 20 cm body length and weight of 3.1 kg developed by *Fukuoka* and *Kimura* [16.62]. It can walk on irregular terrain by using a controller based on a central pattern generator (CPG) and reflex controls.

BigDog is an energy-autonomous hydraulic quadruped robot that is 1 m tall and 1 m long, and weighs 90 kg, developed by *Buehler* et al., (Fig. 16.35b). Each leg has one passive linear pneumatic compliance in the lower leg, and three active joints for knee, hip pitch, and roll [16.63]. In an outdoor environment, BigDog can walk up and down 35° inclines, can trot at speeds of up to 0.8 m/s, and can carry over 50 kg of payload.

16.5.4 Behavior-Based Multilegged Robots

Figure 16.36a shows a small hexapod robot Genghis (35 cm length and 1 kg weight) developed by *Brooks* [16.64]. Most importantly, the gait of Genghis was not explicitly controlled, but emerged from the carefully designed network named *subsumption architecture*. Genghis and other robots created by Brooks created a huge trend of *behavior-based robotics* in robotics and artificial intelligence in the 1990s.

Figure 16.36b shows the eight-legged robot SCORPION (65 cm length and 11.5 kg weight) developed in collaboration between the University of Bremen and the National Aeronautics and Space Administration (NASA) [16.65]. The gait control of SCORPION is designed based on a behavior-based network and a central pattern generator.

16.6 Other Legged Robots

16.6.1 Leg–Wheel Hybrid Robots

Unlike animals or insects, a robot can be designed to have wheels that can rotate infinitely. By mixing the efficiency of wheels and the flexibility of legs, we can expect a robot of maximum terrain adaptivity with minimum power consumption. Figure 16.37 shows examples of such design concept.

Figure 16.37a shows stair climbing by a biped leg–wheeled robot developed by *Matsumoto* et al. [16.70]. The robot is a planer biped with telescopic legs, but the tip of each leg is equipped with a powered wheel. During the single-leg support phase, the robot is controlled as a wheeled inverted pendulum. In addition, a controller was developed to realize a smooth transient between the single support and statically stable double support phases.

Figure 16.37b shows RollerWalker, developed by *Hirose* et al. [16.71,76]. RollerWalker is a 12-DOF quadruped robot equipped with passive wheels on the tip of legs. It uses a roller-skating mode on a flat floor, while it can walk on an uneven terrain by retracting the passive wheels.

Figure 16.37c shows RHex developed by *Buehler* et al. [16.72]. Although it was originally inspired from the locomotion of cockroach, RHex has only six active DOF, that is, one actuator for each hip. Moreover, the legs can rotate full circle around the pitch axis. Using this unique design, RHex can walk and run over rugged, broken, and obstacle-ridden ground. Recently, it also demonstrated biped running with its rear legs [16.77].

Figure 16.37d shows Whegs II, another cockroach-inspired robot developed by *Allen* et al. [16.73]. This robot has only four active DOFs, one for propulsion, two for steering, and one for body flexion. Each leg is equipped with three spring-loaded spokes and is driven by the same actuator. Whegs II can realize comparable mobility to RHex, while it uses fewer actuators.

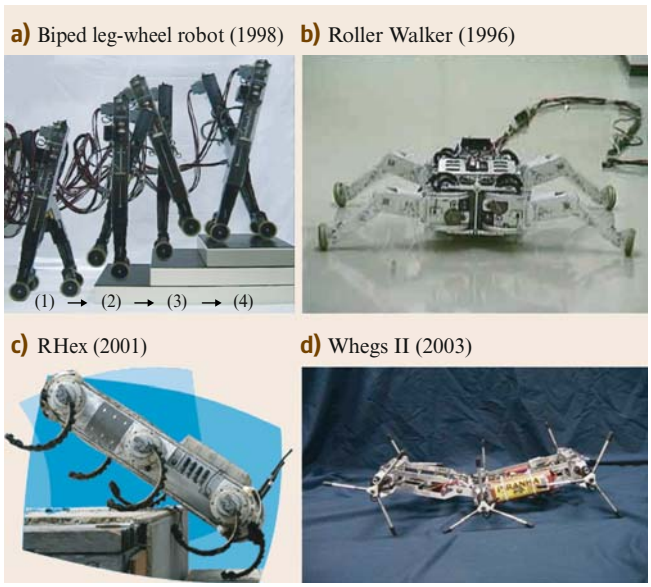

Fig. 16.37a–d Leg–wheel hybrid robots [16.70–73]

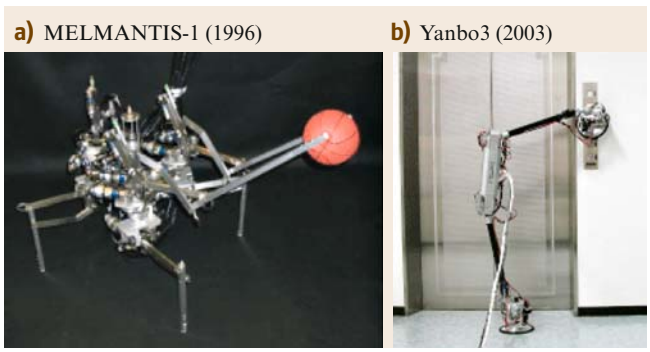

Fig. 16.38a,b Leg–arm hybrid robots [16.74, 75]

Fig. 16.39 Dante II (1994) [16.78]

a) NINJA-1 (1991) **b)** RiSE (2005)

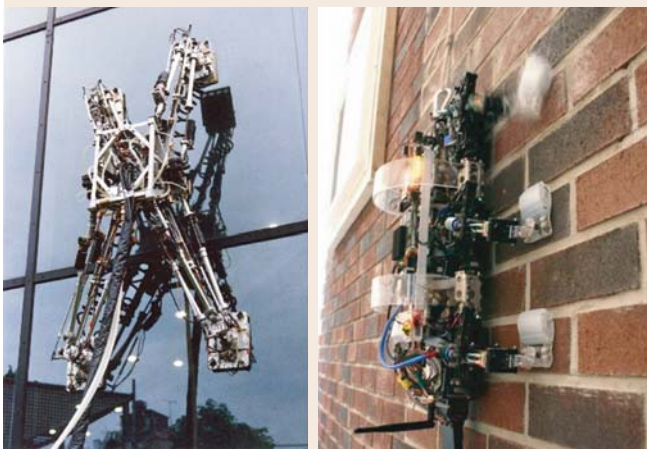

Fig. 16.40a,b Wall-climbing robots [16.79, 80]

16.6.2 Leg–Arm Hybrid Robots

Another design concept is the leg–arm hybrid robot. Since legs have inherently many degree of freedom, it is possible to use them as manipulators. In this way, we can minimize the total number of DOFs, complexity, weight, and power consumption of the walking robot. MELMANTIS-1 (Fig. 16.38a) developed by *Koyachi* et al. is a hexapod walker with 22 DOFs that can transform its legs into manipulators [16.74]. The robot can manipulate an object using two legs while standing with four other legs, after traveling on six legs for maximum stability.

Yanbo3 is a biped walker with eight DOFs developed by the group of *Yoneda* and *Hirose* [16.75]. It is designed to have the minimum number of DOFs necessary for a biped robot as well as for a manipulator when it is in the single support phase. In Fig. 16.38b, the robot is pressing the elevator button using its foot.

16.6.3 Tethered Walking Robots

Figure 16.39 shows Dante II, an eight-legged tethered walking robot developed by the eCMU Field Robotics Center in 1994. It was used at an Alaskan volcano for scientific exploration. To descend down steep crater walls in a rappelling-like manner, the robot uses a tether cable anchored at the crater rim [16.78]. *Hirose* et al. also developed a tethered quadruped for construction work [16.81].

16.6.4 Wall-Climbing Robots

Wall-climbing robots are characterized by their foot mechanisms and leg configurations. The vital part is the foot mechanism to generate the pulling force, and the use of vacuum suction cups, electromagnets (for steel wall), adhesive materials, or miniature spine array have been proposed.

Figure 16.40a shows the wall-climbing quadruped NINJA-1 developed by *Hirose* et al. [16.79]. Each foot of NINJA-1 is equipped with a specially designed suction pad that can minimize its vacuum leakage. Another reliable wall-climbing robot with suction cups was developed by *Yano* et al. [16.82].

Figure 16.40b shows the wall-climbing hexapod RiSE developed by *Kim* et al. [16.80, 83]. Each foot of RiSE is equipped with arrays of miniature spines observed in some insects and spiders. The robot can reliably climb on a wide variety of outdoor surfaces including concrete, stucco, brick, and dressed sandstone.

16.7 Performance Indices

In this section, we introduce useful performance indices that can be used to evaluate legged robots of different configurations.

16.7.1 Expansion of the Stability Margin Concept

As we see in Sect. 16.5.1, the stability margin was originally proposed for a degree of stability of the static walking multilegged robots by *McGhee* and *Frank* [16.57]. For a dynamic walking robot, we can define a stability margin as the minimum distance of the ZMP to the boundaries of the support polygon, since the ZMP is the natural extension of a projected CoM on the ground. This fact was already mentioned in the original work on the ZMP [16.36], and has been used implicitly by many researchers. Explicit definition of this *ZMP stability margin* can be seen, for example, in *Huang* et al. [16.41].

For a legged robot on rough terrain, Messuri and Klein defined the *energy stability margin* as the minimum potential energy required to tumble the robot as,

$$S_{\mathrm{E}} = \min_i (Mgh_i)\,, \tag{16.56}$$

where h_i is the CG height variation during the tumble around the i-th segment of the support polygon and M is the total mass of the robot [16.85]. This concept is widely accepted, and there are some proposals for improvement [16.31, 86].

16.7.2 Duty Factor and Froude Number

Throughout this chapter, we have observed various walking robots that might fit best for certain environments and purposes. In some cases, however, we need to compare walking robots which have different masses,

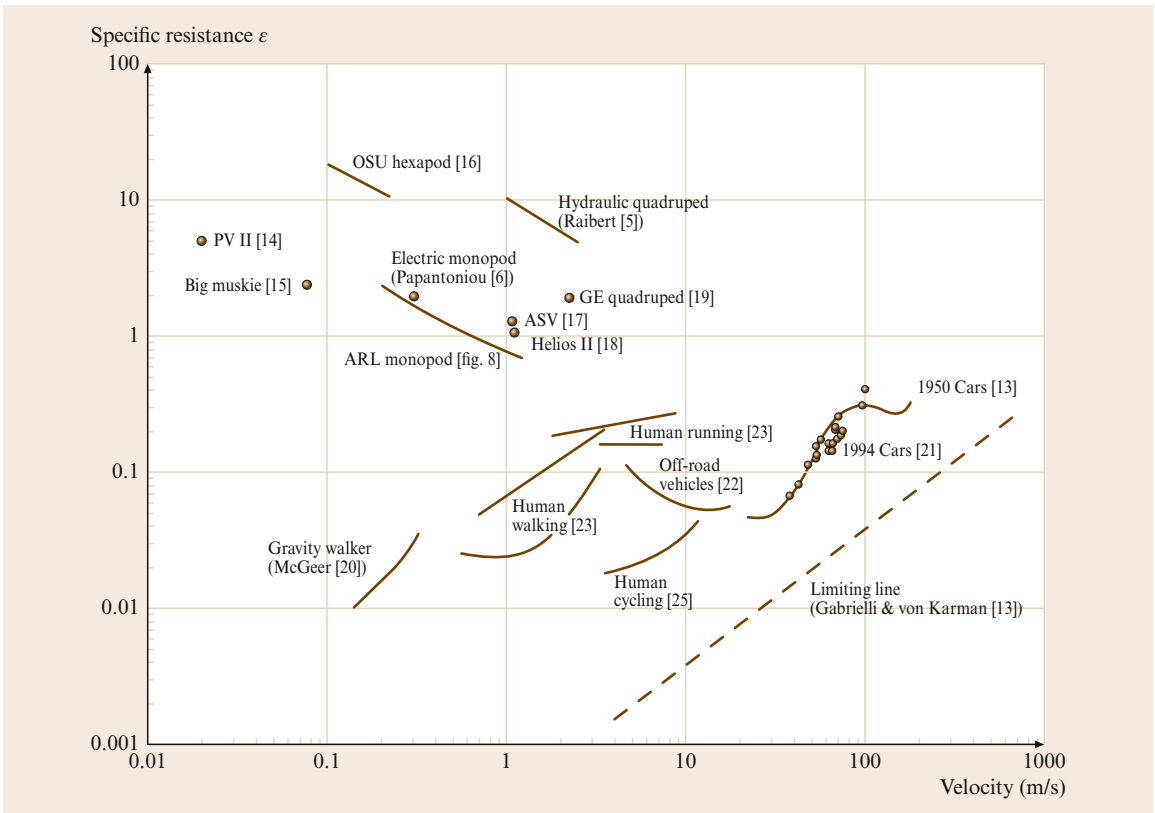

Fig. 16.41 The Gabrielli–von Karman diagram [16.84]

sizes, and numbers of legs by using a certain performance index. Such an index should be dimensionless like a Mach or Reynolds number in fluid mechanics.

One of the useful indices for walking machines was already shown, that is, the duty factor β defined as

$$\beta = \frac{(\text{support period})}{(\text{cycle time})} .$$

Duty factors can be used to make the distinction between walks and runs, since we have $\beta \geq 0.5$ for walking and $\beta < 0.5$ for running [16.67].

The Froude number is used in fluid mechanics to explain the behavior of surface waves. Since both of surface waves and legged locomotion are dynamic motion in gravity, *Alexander* used it to characterize animal locomotion [16.67, 87]. He calculated a Froude number by

$$F_{r_2} = \frac{V^2}{gh} , \tag{16.57}$$

where V is the walking or running speed, g is the acceleration due to gravity, and h is the height of hip joint from the ground. He showed that animals of different sizes use similar gaits when they travel with equal Froude numbers. In particular, most animals change their gait from walking to running at a speed equivalent to a Froude number of $F_{r_2} = 1$.

The Froude number is also defined as

$$F_{r_1} = \frac{V}{\sqrt{gh}}, \tag{16.58}$$

which is the square root of F_{r_2} and can be used as a dimensionless speed for animals or legged robots.

16.7.3 Specific Resistance

The *specific resistance* is another important dimensionless number that is used to evaluate the energy efficiency of a mobile robot.

Gabrielli and von Karman discussed the performance of various vehicles using the power consumption per unit distance. That is

$$\epsilon = \frac{E}{Mgd} , \tag{16.59}$$

where E is the total energy consumption for a travel of distance d, M is the total mass of the vehicle, and g is the acceleration due to gravity [16.88]. Note that when we push a box of mass M a distance d on a floor with friction coefficient μ, we consume the energy $Mg\mu d$ and the specific resistance becomes $\epsilon = \mu$. Therefore, we can say that the specific resistance indicates how smooth the locomotion is.

In their original work, Gabrielli and von Karman plotted the specific resistance as a function of speed for various vehicles as Fig. 16.41. This is called the *Gabrielli–von Karman diagram* and it was used to compare various styles of locomotion by *Umetani* and *Hirose* [16.89]. *Gregorio*, *Ahmadi* and *Buehler* also showed the specific resistance of recent walking robots including their efficient hopping robot, ARL monopod [16.84].

16.8 Conclusions and Future Trends

In this chapter, we have discussed the following topics.

Sect. 16.1 *A brief history:* The history of legged robot research was introduced.

Sect. 16.2 *Analysis of cycling walking:* As the typical cycling walking robot, a simple passive walker was analyzed. The Poincaré map is one of the most important tools for this purpose.

Sect. 16.3 *Control of biped robots using forward dynamics:* The dynamics and control of biped robots were discussed. The treatment of the unilateral ground force is the key issue for bipeds, as well as other legged robots.

Sect. 16.4 *Biped robots in the ZMP scheme:* As a practical scheme to control biped robots, the zero-moment point (ZMP) was discussed.

Sect. 16.5 *Multilegged robots:* The relationship between gaits and stability was discussed. In addition, the landmark robots in this field were introduced.

Sect. 16.6 *Other legged robots:* We introduced leg–wheel hybrid, leg–arm hybrid, tethered walking, and wall-climbing robots. One might be impressed with the range of imagination displayed here, but these examples are still just the tip of the iceberg.

Sect. 16.7 *Performance indices:* The stability margin, Froude number, and the specific resistance were discussed. They are useful performance indices to compare legged robots in different configurations.

Over the last three decades, legged robots have become faster, more efficient, and more robust. This trend may continue in the future, aiming for ultimate mobility comparable to that of insects, mammals, and ourselves.

References

16.1 M. Wisse, L. Schwab, F.L.T. Van der Helm: Passive walking dynamic model with upper body, Robotica **22**(6), 681–688 (2004)

16.2 C. Chevallereau, G. Abba, Y. Aoustin, F. Plestan, E.R. Westervelt, C. Canudas-de-Wit, J.W. Grizzle: RABBIT: a testbed for advanced control theory, IEEE Contr. Syst. Mag. **23**(5), 57–79 (2003)

16.3 M. Vukobratović, B. Borovac: Zero-moment point – Thirty five years of its life, Int. J. Humanoid Robot. **1**(1), 157–173 (2004)

16.4 T. McGeer: Passive dynamic walking, Int. J. Robot. Res. **9**(2), 62–82 (1990)

16.5 M.H. Raibert: *Legged Robots That Balance* (MIT Press, Cambridge 1986)

16.6 M. Coleman, A. Ruina: An uncontrolled walking toy that cannot stand still, Phys. Rev. Lett. **80**(16), 3658–3661 (1998)

16.7 A. Goswami, B. Thuilot, B. Espiau: A study of a compass-like biped robot: symmetry and chaos, Int. J. Robot. Res. **17**(12), 1282–1301 (1998)

16.8 C. Azevedo, B. Amblard, B. Espiau, C. Assaiante: A synthesis of bipedal locomotion in human and robots, Res. Rep. 5450, INRIA https://hal.inria.fr/inria-00070557 (December 2004)

16.9 C. Azevedo, B. Espiau, B. Amblard, C. Assaiante: Bipedal locomotion: toward unified concepts in robotics and neurosciences, Biol. Cybern. **96**(2), 209–228 (2007)

16.10 P.B. Wieber: Constrained stability and parameterized control in biped walking, Int. Symp. Math. Theory Netw. Syst. (2000)

16.11 P.B. Wieber: On the stability of walking systems, Int. Workshop Humanoids Human Friendly Robot. (2002)

16.12 F. Pfeiffer, C. Glocker: *Multibody Dynamics with Unilateral Contacts* (Wiley, New York 1996)

16.13 L. Righetti, A.J. Ijspeert: Programmable central pattern generators: an application to biped locomotion control, IEEE Int. Conf. Robot. Autom. (Orlando,USA May 2006)

16.14 K. Matsuoka: Sustained oscillations generated by mutually inhibiting neurons with adaptation, Biol. Cybern. **52**, 345–353 (1985)

16.15 G. Endo, J. Morimoto, J. Nakanishi, G. Cheng: An empirical exploration of a neural oscillator for biped locomotion control, IEEE Int. Conf. Robot. Autom. (New Orleans 2004) pp. 3036–3042

16.16 D.C. Witt: A feasibility study on powered lower-limb prosthesis, Univer. Oxford Dep. Eng. Sci. Rep. (1970)

16.17 F. Gubina, H. Hemami, R.B. McGhee: On the dynamic stability of biped locomotion, IEEE Trans. Biomed. Eng. **BME-21**(2), 102–108 (1974)

16.18 H. Miura, I. Shimoyama: Dynamic walk of a biped, The Int. J. Robot. Res. **3**(2), 60–74 (1984)

16.19 J. Furusho, M. Masubuchi: A theoretically motivated reduced order model for the control of dynamic biped locomotion, J. Dyn. Syst. Meas. Contr. **109**, 155–163 (1987)

16.20 S. Kawamura, F. Miyazaki, S. Arimoto: Realization of robot motion based on a learning method, IEEE Trans. Syst. Man Cybern. **18**(1), 126–134 (1988)

16.21 S. Kajita, T. Yamaura, A. Kobayashi: Dynamic walking control of a biped robot along a potential energy conserving orbit, IEEE Trans. Robot. Autom. **8**(4), 431–438 (1992)

16.22 J. Pratt, C.-M. Chew, A. Torres, P. Dilworth, G. Pratt: An intuitive approach for bipedal locomotion, Int. J. Robot. Res. **20**(2), 129–143 (2001)

16.23 E.R. Westervelt, J.W. Grizzle, D.E. Koditschek: Hybrid zero dynamics of planar biped walkers, IEEE Trans. Autom. Contr. **48**(1), 42–56 (2003)

16.24 S. Lohmeier, K. Löffler, M. Gienger, H. Ulbrich, F. Pfeiffer: Computer system and control of biped Johnnie, IEEE Int. Conf. Robot. Autom. (New-Orleans 2004) pp. 4222–4227

16.25 J.H. Kim, J.H. Oh: Walking control of the humanoid platform KHR-1 based on torque feedback control, IEEE Int. Conf. Robot. Autom. (2004) pp. 623–628

16.26 P.B. Wieber, C. Chevallereau: Online adaptation of reference trajectories for the control of walking systems, Robot. Auton. Syst. **54**(7), 559–566 (2006)

16.27 F. Allgöwer, T.A. Badgwell, J.B. Rawlings, S.J. Wright: Nonlinear predictive control and moving horizon estimation an overview., Eur. Contr. Conf. (Karlsruhe 1999) pp. 392–449

16.28 C. Azevedo, P. Poignet, B. Espiau: Artificial locomotion control: from human to robots, Robot. Auton. Syst. **47**(4), 203–223 (2004)

16.29 P.B. Wieber: Trajectory-free linear model predictive control for stable walking in the presence

of strong perturbations, IEEE-RAS Int. Conf. Humanoid Robots (Genoa 2006)
16.30 A. Takanishi, M. Ishida, Y. Yamazaki, I. Kato: The realization of dynamic walking by the biped walking robot WL-10RD, Int. Conf. Adv. Robot. (ICAR'85) (1985) pp. 459–466
16.31 M. Hirose, Y. Haikawa, T. Takenaka, K. Hirai: Development of humanoid robot ASIMO, IEEE/RSJ Int. Conf. Intell. Robots Syst. – Workshop 2 (2001)
16.32 M. Gienger, K. Löffler, F. Pfeiffer: Towards the design of a biped jogging robot, IEEE Int. Conf. Robot. Autom. (2001) pp. 4140–4145
16.33 K. Kaneko, S. Kajita, F. Kanehiro, K. Yokoi, K. Fujiwara, H. Hirukawa, T. Kawasaki, M. Hirata, T. Isozumi: Design of advanced leg module for humanoid robotics project of METI, IEEE Int. Conf. Robot. Autom. (2002) pp. 38–45
16.34 Y. Sugahara, M. Kawase, Y. Mikuriya, T. Hosobata, H. Sunazuka, K. Hashimoto, H. Lim, A. Takanishi: Support torque reduction mechanism for biped locomotor with parallel mechanism, IEEE/RSJ Int. Conf. Intell. Robots Syst. (2004) pp. 3213–3218
16.35 I.W. Park, J.Y. Kim, J. Lee, J.H. Oh: Online free walking trajectory generation for biped humanoid robot KHR-3(HUBO), IEEE Int. Conf. Robot. Autom. (Orlando 2006) pp. 1231–1236
16.36 M. Vukobratović, J. Stepanenko: On the stability of anthropomorphic systems, Math. Biosci. **15**, 1–37 (1972)
16.37 S. Kajita, F. Kanehiro, K. Kaneko, K. Fujiwara, K. Harada, K. Yokoi, H. Hirukawa: Biped walking pattern generation by using preview control of zero-moment point, IEEE Int. Conf. Robot. Autom. (2003) pp. 1620–1626
16.38 A. Takanishi, Y. Egusa, M. Tochizawa, T. Takeya, I. Kato: Realization of dynamic biped walking stabilized with trunk motion, ROMANSY 7 (1988) pp. 68–79
16.39 A. Takanishi, H. Lim, M. Tsuda, I. Kato: Realization of dynamic biped walking stabilized by trunk motion on a sagittally uneven surface, IEEE Int. Workshop Intell. Robots Syst. (1990) pp. 323–330
16.40 S. Kagami, K. Nishiwaki, T. Kitagawa, T. Sugihiara, M. Inaba, H. Inoue: A fast generation method of a dynamically stable humanoid robot trajectory with enhanced ZMP constraint, IEEE Int. Conf. Humanoid Robot. (2000)
16.41 Q. Huang, K. Yokoi, S. Kajita, K. Kaneko, H. Arai, N. Koyachi, K. Tanie: Planning walking patterns for a biped robot, IEEE Trans. Robot. Autom. **17**(3), 280–289 (2001)
16.42 T. Sugihara, Y. Nakamura, H. Inoue: Realtime humanoid motion generation through ZMP manipulation based on inverted pendulum control, IEEE Int. Conf. Robot. Autom. (2002) pp. 1404–1409
16.43 K. Nagasaka, K. Kuroki, S. Suzuki, Y. Itoh, J. Yamaguchi: Integrated motion control for walking, jumping and running on a small bipedal entertainment robot, IEEE Int. Conf. Robot. Autom. (2004) pp. 3189–3194
16.44 K. Harada, S. Kajita, F. Kanehiro, K. Fujiwara, K. Kaneko, K. Yokoi, H. Hirukawa: Real-time planning of humanoid robot's gait for force controlled manipulation, IEEE Int. Conf. Robot. Autom. (2004) pp. 616–622
16.45 M. Tomizuka, D.E. Rosenthal: On the optimal digital state vector feedback controller with integral and preview actions, Trans. the ASME J. Dyn. Syst. Meas. Contr. **101**, 172–178 (1979)
16.46 T. Katayama, T. Ohki, T. Inoue, T. Kato: Design of an optimal controller for a discrete time system subject to previewable demand, Int. J. Contr. **41**(3), 677–699 (1985)
16.47 J. Yamaguchi, A. Takanishi, I. Kato: Experimental development of a foot mechanism with shock absorbing material for acquisition of landing surface position information and stabilization of dynamic biped walking, IEEE Int. Conf. Robot. Autom. (1995) pp. 2892–2899
16.48 K. Hirai, M. Hirose, Y. Haikawa, T. Takenaka: The development of honda humanoid robot, IEEE Int. Conf. Robot. Autom. (1998) pp. 1321–1326
16.49 K. Yokoi, F. Kanehiro, K. Kaneko, S. Kajita, K. Fujiwara, H. Hirukawa: Experimental study of humanoid robot HRP-1S, Int. J. Robot. Res. **23**(4-5), 351–362 (2004)
16.50 K. Hashimoto, Y. Sugahara, H. Sunazuka, C. Tanaka, A. Ohta, M. Kawase, H. Lim, A. Takanishi: Biped landing pattern modification method with nonlinear compliance control, IEEE Int. Conf. Robot. Autom. (Orlando 2006) pp. 1213–1218
16.51 A. Goswami: Postural stability of biped robots and the foot-rotation indicator(FRI) point, Int. J. Robot. Res. **18**(6), 523–533 (1999)
16.52 P. Sardain, G. Bessonnet: Forces acting on a biped robot. center of pressure–zero moment point, IEEE Trans. Syst. Man Cybern. Part A: Syst. Humans **34**(5), 630–637 (2004)
16.53 T. Saida, Y. Yokokoji, T. Yoshikawa: FSW (feasible solution of wrench) for multi-legged robots, IEEE Int. Conf. Robot. Autom. (2003) pp. 3815–3820
16.54 H. Hirukawa, S. Hattori, K. Harada, S. Kajita, K. Kaneko, F. Kanehiro, K. Fujiwara, M. Morisawa: A universal stability criterion of the foot contact of legged robots – Adios ZMP, IEEE Int. Conf. Robot. Autom. (Orlando 2006), pp. 1976–1983
16.55 R.B. McGhee: Vehicular legged locomotion. In: *Advances in Automation and Robotics*, ed. by G.N. Saridis (JAI Press, New York 1985) pp. 259–284
16.56 S.M. Song, K.J. Waldron: *Machines that Walk: the Adaptive Suspension Vehicle* (The MIT Press, Cambridge 1989)
16.57 R.B. McGhee, A.A. Frank: On the stability properties of quadruped creeping gaits, Math. Biosci. **3**, 331–351 (1968)

16.58 K.J. Waldron, R.B. McGhee: The adaptive suspension vehicle, IEEE Contr. Syst. Mag. **6**, 7–12 (1986)

16.59 S. Hirose, Y. Fukuda, H. Kikuchi: The gait control system of a quadruped walking vehicle, Adv. Robot. **1**(4), 289–323 (1986)

16.60 S. Hirose, K. Yoneda, R. Furuya, T. Takagi: Dynamic and static fusion control of quadruped walking vehicle, IEEE/RSJ Int. Workshop Intell. Robots Syst. (1989) pp. 199–204

16.61 S. Hirose: A study of design and control of a quadruped walking vehicle, Int. J. Robot. Res. **3**(2), 113–133 (1984)

16.62 Y. Fukuoka, H. Kimura, A.H. Cohen: Adaptive dynamic walking of a quadruped robot on irregular terrain based on biological concepts, Int. J. Robot. Res. **22**(3-4), 187–202 (2003)

16.63 M. Buehler, R. Playter, M. Raibert: Robots step outside, Int. Symp. Adapt. Motion Animals Mach. (AMAM) (Ilmenau 2005)

16.64 R.A. Brooks: A robot that walks; emergent behavior from a carefully evolved network, IEEE Int. Conf. Robot. Autom. (Scottsdale 1989) pp. 292–296

16.65 D. Spenneberg, K. McCullough, F. Kirchner: Stability of walking in a multilegged robot suffering leg loss, IEEE Int. Conf. Robot. Autom. (2004) pp. 2159–2164

16.66 S. Hirose, K. Yoneda, K. Arai, T. Ibe: Design of prismatic quadruped walking vehicle TITAN VI, 5th Int. Conf. Adv. Robot. (Pisa taly 1991) pp. 723–728

16.67 R. McNeill Alexander: The gait of bipedal and quadrupedal animals, Int. J. Robot. Res. **3**(2), 49–59 (1984)

16.68 H. Kimura, I. Shimoyama, H. Miura: Dynamics in the dynamic walk of a quadruped robot, Adv. Robot. **4**(3), 283–301 (1990)

16.69 J. Furusho, A. Sano, M. Sakaguchi, E. Koizumi: Realization of bounce gait in a quadruped robot with articular-joint-type legs, IEEE Int. Conf. Robot. Autom. (1995) pp. 697–702

16.70 O. Matsumoto, S. Kajita, M. Saigo, K. Tani: Dynamic trajectory control of passing over stairs by a biped type leg-wheeled robot with nominal reference of static gait, IEEE/RSJ Int. Conf. Intell. Robot Syst. (1998) pp. 406–412

16.71 S. Hirose, H. Takeuchi: Study on roller-walk (basic characteristics and its control), IEEE Int. Conf. Robot. Autom. (1996) pp. 3265–3270

16.72 U. Saranli, M. Buehler, D.E. Koditschek: RHex: a simple and highly mobile hexapod robot, Int. J. Robot. Res. **20**(7), 616–631 (2001)

16.73 T.J. Allen, R.D. Quinn, R.J. Bachmann, R.E. Ritzmann: Abstracted biological principles applied with reduced actuation improve mobility of legged vehicles, IEEE Int. Conf. Intell. Robots Syst. (Las Vegas 2003) pp. 1370–1375

16.74 N. Koyachi, H. Adachi, M. Izumi, T. Hirose, N. Senjo, R. Murata, T. Arai: Multimodal control of hexapod mobile manipulator MELMANTIS-1, 5th Int. Conf. Climbing Walking Robots (2002) pp. 471–478

16.75 Y. Ota, T. Tamaki, K. Yoneda, S. Hirose: Development of walking manipulator with versatile locomotion, IEEE Int. Conf. Robot. Autom. (2003) pp. 477–483

16.76 G. Endo, S. Hirose: Study on roller-walker: system integration and basic experiments, IEEE Int. Conf. Robot. Autom. (Detroit 1999) pp. 2032–2037

16.77 N. Neville, M. Buehler, I. Sharf: A bipedal running robot with one actuator per leg, IEEE Int. Conf. Robot. Autom. (Orlando 2006) pp. 848–853

16.78 J. Bares, D. Wettergreen: Dante II: technical description, results and lessons learned, Int. J. Robot. Res. **18**(7), 621–649 (1999)

16.79 S. Hirose, A. Nagakubo, R. Toyama: Machine that can walk and climb on floors, walls and ceilings, 5th Int. Conf. Adv. Robot. (Pisa 1991) pp. 753–758

16.80 S. Kim, A. Asbeck, W. Provancher, M.R. Cutkosky: SpinybotII: Climbing hard walls with compliant microspines, IEEE ICAR (Seattle 2005) pp. 18–20

16.81 S. Hirose, K. Yoneda, H. Tsukagoshi: TITAN VII: quadruped walking and manipulating robot on a steep slope, IEEE Int. Conf. Robot. Autom. (1997)

16.82 T. Yano, S. Numao, Y. Kitamura: Development of a self-contained wall climbing robot with scanning type suction cups, IEEE/RSJ Int. Conf. Intell. Robots Syst. (1998) pp. 249–254

16.83 A.T. Asbeck, S. Kim, A. McClung, A. Parness, M.R. Cutkosky: Climbing walls with microspines (video), IEEE Int. Conf. Robot. Autom. (Orlando 2006)

16.84 P. Gregorio, M. Ahmadi, M. Buehler: Design, control, and energetics of an electrically actuated legged robot, IEEE Trans. Syst. Man Cyber. – Part B: Cyber. **27**(4), 626–634 (1997)

16.85 D.A. Messuri, C.A. Klein: Automatic body regulation for maintaining stability of a legged vehicle during rough-terrain locomotion, IEEE J. Robot. Autom. **RA-1**(3), 132–141 (1985)

16.86 E. Garcia, P. Gonzalez de Santos: An improved energy stability margin for walking machines subject to dynamic effects, Robotica **23**(1), 13–20 (2005)

16.87 R. McNeill Alexander: *Exploring Biomechanics – Animals in Motion* (W.H. Freeman, New York 1992)

16.88 G. Gabrielli, T. von Karman: What price speed – specific power required for propulsion of vehicles, Mech. Eng. **72**(10), 775–781 (1950)

16.89 Y. Umetani, S. Hirose: Biomechanical study of serpentine locomotion (evaluation as a locomotion measure) (in Japanese). In: *BIOMECHANISM(2)* (Univ. Tokyo Press, Tokyo 1973) pp. 289–297